TRANSVERSE CRACKING IN A FIBER REINFORCED CERAMIC MATRIX COMPOSITE

THESIS

Steven E. Bachmann
Captain, USAF

AFIT/GAE/ENY/90D-2

DEPARTMENT OF THE AIR FORCE
AIR UNIVERSITY
AIR FORCE INSTITUTE OF TECHNOLOGY

Wright-Patterson Air Force Base, Ohio

AFIT/GAE/ENY/90D-2

TRANSVERSE CRACKING IN A FIBER REINFORCED CERAMIC MATRIX COMPOSITE

THESIS

Steven E. Bachmann
Captain, USAF

AFIT/GAE/ENY/90D-2

AFIT/GAE/ENY/90D-2

TRANSVERSE CRACKING IN A FIBER REINFORCED CERAMIC MATRIX COMPOSITE

THESIS

Presented to the Faculty of the School of Engineering

of the Air Force Institute of Technology

Air University

In Partial Fulfillment of the

Requirements for the Degree of

Master of Science in Aeronautical Engineering

Steven E. Bachmann
Captain, USAF

December 1990

Preface

The purpose of this study was to investigate the effects of laminate geometry on transverse cracking in a fiber reinforced ceramic matrix composite. The primary focus was to gain an understanding of the correlation between crack initiation stress, crack density and transverse ply thickness in cross-ply laminates.

Four different lay-ups ($0_3/90/0_3$, $0_3/90_2/0_3$, $0_3/90_3/0_3$, and $0/90/0_4/90/0$) were tested in uni-axial tension. Acoustic emission and replication were used to monitor crack initiation and progression. The test results were compared with the existing theoretical modeling techniques for the behavior of composite materials. The cracking behavior of the ceramic matrix composite was compared to glass/epoxy and graphite/epoxy systems.

Throughout this endeavor I have received a great deal of assistance, encouragement and support from numerous individuals. Firstly I would like to thank my advisor, Dr. Shankar Mall, for his guidance, patience and gentle prodding without which this project would have been much more painful. I am also thankful for the help of the lab technicians, Jay Anderson and Mark Derriso. Much thanks goes to Dr. Nicholas and Mr. Larry Zawada of WRDC/MLLN for their sponsorship and the use of their facilities and to Ron Trejo of UDRI for his help with the acoustic emission. Most of all, I wish to

thank my wife Julianna for her endless encouragement, patience and understanding during our time at AFIT.

Steven E. Bachmann

Table of Contents

List of Figures

List of Tables

Abstract

The purpose of this study was to investigate the transverse cracking behavior of a fiber reinforced ceramic matrix composite, SiC/1723. The major objectives were: (1) to determine the crack initiation stress and the minimum transverse crack spacing for different cross-ply lay-ups of SiC/1723, (2) to provide explanation for the differences in the performance of the lay-ups, and (3) to compare the test results to available theoretical models and to other composite systems.

Four different cross-ply lay-ups ($0_3/90/0_3$, $0_3/90_2/0_3$, $0_3/90_3/0_3$, and $0/90/0_4/90/0$) were tested in uni-axial tension. Acoustic emission was used during testing to assist in crack detection. A series of replications were taken of each specimen at different load levels up to failure. These replications were used to determine the stress level for crack initiation and also the transverse crack spacing as a function of stress and strain.

Transverse cracking developed in the 90° plies at relatively low stress levels. The cracks generally formed at the 0°/90° ply interface and progressed straight through the 90° ply, perpendicular to the direction of the applied load As the applied load was increased more cracks formed, evenly spaced along the length of the 90° ply. After a certain

amount of loading the specimens reached a crack saturation level, after which an increase in the load did not result in any new transverse cracks.

The thickness of the transverse ply was found to have a great effect on the transverse cracking behavior of the laminates. The saturation crack spacing decreased (i.e., the cracks were closer together) as the transverse ply thickness was decreased and for a given strain, the crack spacing increased as the transverse ply thickness was increased. The strain for the onset of transverse cracking increased as the transverse ply thickness was decreased.

Classical laminate theory was used to predict crack initiation stresses and modulus of elasticity values. A crack spacing theory based on shear lag analysis was applied. While the observed crack spacing was always higher than that predicted by the theory, the theory was useful in predicting general crack spacing trends.

Saturation crack spacing in SiC/1723 was shown to follow the same trends as in glass/epoxy and graphite/epoxy. However, because of its brittle matrix, transverse cracking in SiC/1723 begins at a much lower strain than in glass/epoxy or graphite/epoxy.

TRANSVERSE CRACKING IN A FIBER REINFORCED CERAMIC MATRIX COMPOSITE

I. Introduction

Composite materials have a long history of usage. While their beginnings are unclear, early recorded history does contain references to some forms of composite materials. For example, the Israelites added straw to mud to produce a stronger brick. The Egyptians discovered that by arranging layers of wood in particular directions they could achieve greater strength and resistance to thermal expansion. Thus, plywood was invented. More recently, fiber reinforced resin composites have found wide applications in weight sensitive areas such as aircraft and space structures because of their high strength-to-weight and stiffness-to-weight ratios. As the desired specific thrust of jet engines continues to increase and as hypervelocity aircraft such as the National Aerospace Plane are developed, the need for high strength materials that can operate at high temperatures will become critical. Many ceramics and glasses possess high strength at high temperature. However, they also have low fracture toughness. One way to increase the toughness of the ceramic or glass is to reinforce it with a high strength fiber. A

fiber reinforced ceramic matrix composite usually consists of strong fibers surrounded by weaker matrix material which protects the fibers, binds the fibers together and transfers the load between the fibers. Continuous fiber reinforced ceramic matrix composites generally exhibit non-brittle failure behavior along with increased strength and toughness.

Matrix cracking in off-axis plies of continuous fiber reinforced composite laminates has been a subject of considerable research for over a decade. This matrix cracking is commonly referred to as transverse cracking. As the off-axis plies of a laminate are subjected to a monotonically increasing load, the number of transverse cracks increases until a saturation spacing is reached. The load in a cracked ply is transferred to the adjacent plies and is reintroduced into the cracked ply over a distance which is dependent on the stiffness of the cracked and adjacent plies. When the stress in the cracked ply, at some distance away from the crack, reaches the level of stress required to crack the matrix, a second crack will form. This process continues with increasing load until the cracks develop a regular spacing along the length of the ply. The stress level at which the first crack appears and the saturation crack spacing are heavily dependent on the thickness of the off-axis plies.

This study was undertaken in order to better understand the correlation between crack initiation, saturation crack

spacing and off-axis ply thickness in a ceramic matrix composite. This area has been under a great deal of investigation in polymer based composites, but few studies are available in ceramic composites. Thus, there is a need for more such investigations with fiber reinforced ceramics. The chosen composite was SiC/1723, which consists of silicon carbide fibers and a ceramic matrix. The SiC/1723, which is a good model material in this class of materials, was fabricated at the Wright Research and Development Center at Wright-Patterson Air Force Base, Ohio.

A. Background

Transverse cracking is an area of much interest in the composite materials field. Garrett and Bailey (1:157-167) were among the first to investigate transverse cracking in cross-ply laminates. They investigated cross-ply laminates of a glass fiber-reinforced polyester and found that the transverse crack spacing decreased with increasing applied stress and increased with increasing transverse ply thickness. Parvizi, Garrett, and Bailey (2:195-201) demonstrated that transverse cracking could be suppressed completely prior to total specimen failure if the off-axis ply was very thin. Wang and Parvizi-Majidi (3) investigated transverse cracking in Nicalon/CAS, a ceramic composite with silicon carbide fibers and calcium aluminosilicate matrix.

They found that the strain for the onset of transverse cracking increased as the transverse ply thickness decreased.

B. Purpose of This Study

This thesis is primarily focused on understanding the correlation between the crack initiation stress, the saturation crack spacing and the off-axis ply thickness in cross-ply laminates of SiC/1723. Specifically, this thesis involves: determination of the crack initiation stress and the minimum transverse crack spacing for different cross-ply lay-ups of SiC/1723; explanation for the differences in the performance of the different lay-ups; and comparison of the test results to available theoretical models and to other composite systems.

C. Approach

Cross-ply specimens of SiC/1723 fiber reinforced ceramic composite were tested under uniaxial tension to analyze transverse cracking behavior. Four different lay-ups were studied: $0_3/90/0_3$, $0_3/90_2/0_3$, $0_3/90_3/0_3$, and $0/90/0_4/90/0$. The first three lay-ups were chosen to study the effect of the transverse ply thickness, while the fourth was used to examine the impact of the location of the 90^o plies. One 4 inch by 4 inch plate of each lay-up was fabricated at the Wright Research and Development Center. From these plates, 0.25 inch wide specimens were cut. The specimens were

polished on one edge in order to take micrographs and replicas of the material. Tensile tests were conducted at room temperature using an Instron testing machine with a cross-head speed of 0.01 inches per minute. Acoustic emission was used during testing to assist in crack detection. A series of replications were taken of each specimen at different load levels up to failure. These replications were used to determine the stress level for crack initiation and also the transverse crack spacing as a function of stress and strain. Mechanical properties were measured in both the longitudinal and transverse directions using strain gages. The results were compared to the present composite material theories, which were developed primarily for polymer-based composites, for first ply failure and transverse crack spacing.

Chapter II will discuss previous investigations of transverse cracking in composite materials and the theoretical models used to predict first ply failure and transverse crack spacing. Chapter III will give a description of the experimental procedure used for testing the specimens. Chapter IV will present discussion and results of the tests and comparison of the test results to the theoretical models and to other composite systems. Finally, Chapters V and VI will offer conclusions and recommendations from this study respectively.

II. Background

Continuous fiber reinforced ceramic matrix composites are members of a class of composites which are referred to as brittle matrix composites (BMC). Ceramic composites are currently receiving a great deal of consideration for use in high temperature structural applications. These materials are characterized by matrices which are stiff compared to the fibers and exhibit relatively low strain to failure. In addition, the fiber-matrix interfacial bonding may be imperfect. Because of the low strain to failure of the matrix, ceramic composites generally exhibit matrix damage well before final failure of the composite (4:799).

In this chapter previous experimental works in crack initiation, crack progression and crack density will be discussed. Also presented are related theoretical models for crack initiation and first ply failure, Young's modulus prediction, and transverse crack density.

A. Experimental Background

Matrix cracking in off-axis plies of continuous fiber reinforced composite laminates has been investigated in several studies over the last decade, primarily with polymer based systems. Garrett and Bailey (1:157-167) were among the first to study transverse cracking in cross-ply laminates.

They analyzed cross-ply laminates of a glass fiber-reinforced polyester and found that transverse cracks occurred in the 90° plies with remarkably even crack spacing. They observed that the cracks formed in a direction perpendicular to the applied stress and parallel to the transverse fibers and generally extended the full width of the transverse plies. The spacing between the cracks was found to depend on the thickness of the transverse ply. For a given strain it was found that the crack spacing increased as the transverse ply thickness was increased. Finally, Garrett and Bailey observed that the average crack spacing eventually reached a limiting value which also was dependent on the transverse ply thickness. These same phenomena were seen by Sun and Jen (5:212-217) and by Reifsnider, Henneke, and Stinchcomb (6:17-51) for graphite/epoxy composites.

Talreja (7:126) studied the effect of transverse ply thickness on the crack initiation strain. He found that strain for crack initiation decreased as the transverse ply thickness increased until a limiting value was reached. He observed that this limiting strain value was the ultimate transverse strain of the 90° ply.

Parvizi, Garrett, and Bailey (2:197-200) demonstrated that the transverse cracking could be suppressed completely prior to total specimen failure if the off-axis ply was very thin.

Wang and Parvizi-Majidi (3) investigated transverse cracking in Nicalon/CAS, a ceramic composite with silicon carbon fibers and calcium aluminosilicate matrix. They found that the strain for the onset of transverse cracking increased as the transverse ply thickness decreased. They also noted that the outer 0° plies exerted some constraint over transverse cracking.

B. Theoretical Models

This section will present the theoretical models that were used in this thesis for predicting the stress level for crack initiation and first ply failure, the Young's modulus of the laminate, and the crack density.

1. Crack Initiation and First Ply Failure Theoretical Model

In cross-ply composite laminates subjected to uni-axial loading, cracking generally begins in the 90° plies well before laminate failure. Garrett and Bailey (1:162) theorized that if the transverse ply has a unique breaking strain, ε_{tu}, and strength σ_{tu}, then the first transverse crack would occur when

$$\sigma_a = E_c \varepsilon_{tu} \tag{1}$$

where σ_a is the stress applied to the laminate and E_c is the Young's modulus of the laminate in the direction of the longitudinal ply fibers.

The stress level for the failure of the entire transverse ply can be predicted by using the classical lamination theory described by Jones (8:147-155). The following section outlines the procedure used by Jones for prediction of the first ply failure stress level for a generic 0/90 cross-ply laminate.

With known values of E_1, E_2 and ν_{12} for a material, then

$$\nu_{21} = \nu_{12}\left[\frac{E_2}{E_1}\right] \tag{2}$$

The stress-strain relations for the laminate can be written

$$\begin{bmatrix} \sigma_1 \\ \sigma_2 \\ \tau_{12} \end{bmatrix} = \begin{bmatrix} Q_{11} & Q_{12} & 0 \\ Q_{12} & Q_{22} & 0 \\ 0 & 0 & Q_{66} \end{bmatrix} \begin{bmatrix} \varepsilon_1 \\ \varepsilon_2 \\ \gamma_{12} \end{bmatrix} \tag{3}$$

where the Q_{ij}, the so-called reduced stiffnesses, are

$$\begin{aligned} Q_{11} &= \frac{E_1}{1 - \nu_{12}\nu_{21}} \\ Q_{12} &= \nu_{21}Q_{11} \\ Q_{22} &= \frac{E_2}{1 - \nu_{12}\nu_{21}} \\ Q_{66} &= G_{12} \end{aligned} \tag{4}$$

Equation (3) relates the stress and strain in the principal material directions. Using the transformed reduced stiffness matrix $[\bar{Q}]$ it is possible to express the stress-strain relations in the xy coordinate system.

$$\begin{Bmatrix} \sigma_x \\ \sigma_y \\ \tau_{xy} \end{Bmatrix} = [\bar{Q}] \begin{Bmatrix} \varepsilon_x \\ \varepsilon_y \\ \gamma_{xy} \end{Bmatrix} \tag{5}$$

in which

$$\begin{aligned}
\bar{Q}_{11} &= Q_{11}\cos^4\theta + 2(Q_{12} + 2Q_{66})\sin^2\theta\cos^2\theta + Q_{22}\sin^4\theta \qquad (6)\\
\bar{Q}_{12} &= (Q_{11} + Q_{22} - 4Q_{66})\sin^2\theta\cos^2\theta + Q_{12}(\sin^4\theta + \cos^4\theta)\\
\bar{Q}_{22} &= Q_{11}\sin^4\theta + 2(Q_{12} + 2Q_{66})\sin^2\theta\cos^2\theta + Q_{22}\cos^4\theta\\
\bar{Q}_{16} &= (Q_{11} - Q_{12} - 2Q_{66})\sin\theta\cos^3\theta + (Q_{12} - Q_{22} + 2Q_{66})\sin^3\theta\cos\theta\\
\bar{Q}_{26} &= (Q_{11} - Q_{12} - 2Q_{66})\sin^3\theta\cos\theta + (Q_{12} - Q_{22} + 2Q_{66})\sin\theta\cos^3\theta\\
\bar{Q}_{66} &= (Q_{11} + Q_{22} - 2Q_{12} - 2Q_{66})\sin^2\theta\cos^2\theta + Q_{66}(\sin^4\theta + \cos^4\theta)
\end{aligned}$$

and θ is the angle between the x-axis and the lamina fiber direction.

Now $[\bar{Q}]$ is used along with the laminate geometry to determine [A] (the extensional stiffness matrix), [B] (the coupling stiffness matrix) and [D] (the bending stiffness matrix). Referring to Figure 1,

$$A_{ij} = \sum_{n=1}^{N} (\bar{Q}_{ij})_n (h_n - h_{n-1}) \tag{7}$$

$$B_{ij} = \frac{1}{2} \sum_{n=1}^{N} (\bar{Q}_{ij})_n (h_n^2 - h_{n-1}^2) \tag{8}$$

$$D_{ij} = \frac{1}{3} \sum_{n=1}^{N} (\bar{Q}_{ij})_n (h_n^3 - h_{n-1}^3) \tag{9}$$

Using [A], [B], and [D], new matrices [D*], [D_1], [B_1], [C_1], and [A_1] are formed as follows:

$$[D^*] = [D] - [B][A^{-1}][B] \tag{10}$$

$$[D_1] = [(D^*)^{-1}] \tag{11}$$

$$[B_1] = -[A^{-1}][B][(D^*)^{-1}] \tag{12}$$

$$[C_1] = -[(D^*)^{-1}][B][A^{-1}] \tag{13}$$

$$[A_1] = [A^{-1}] + [A^{-1}][B][(D^*)^{-1}][B][A^{-1}] \tag{14}$$

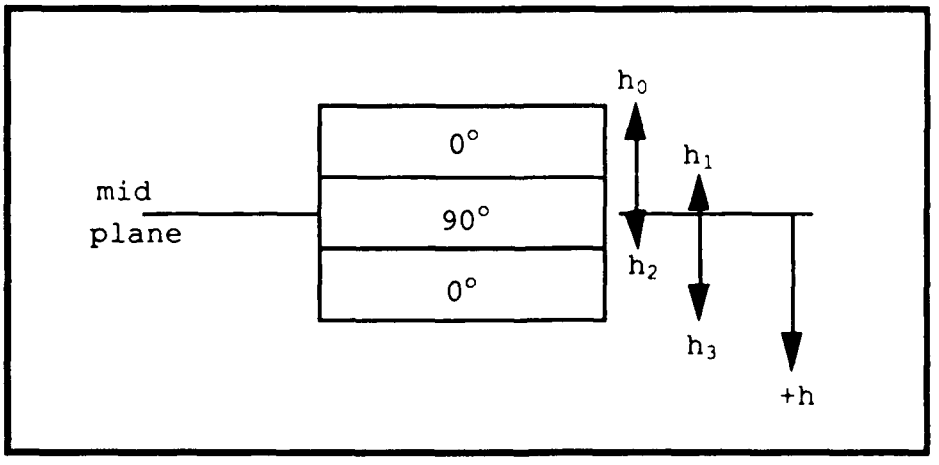

Figure 1. Laminate Geometry

The mid-plane strain of the laminate, $[\varepsilon^0]$, is

$$[\varepsilon^0] = \begin{bmatrix} \varepsilon_x^0 \\ \varepsilon_y^0 \\ \gamma_{xy}^0 \end{bmatrix} = [A_1][N] \tag{15}$$

where [N] is the applied load/thickness. For uniaxial tension,

$$[N] = \begin{bmatrix} N_x \\ 0 \\ 0 \end{bmatrix} \tag{16}$$

When the value of N_x in equation (16) results in a stress in the 90° ply that exceeds the transverse strength of the 90° ply, first ply failure occurs.

The mid-plane curvature $[\kappa]$, is

$$[\kappa] = [C_1][N] \tag{17}$$

The strain at the mid-plane of each lamina is

$$[\varepsilon]_n = \begin{bmatrix} \varepsilon_x \\ \varepsilon_y \\ \gamma_{xy} \end{bmatrix}_n = [\varepsilon^0] - h_n[\kappa] \tag{18}$$

where h_n is the distance from the laminate mid-plane to the lamina mid-plane. With the mid-plane strain known for each lamina as a function of N_x, the stress in each lamina is

$$[\sigma]_n = \begin{bmatrix} \sigma_x \\ \sigma_y \\ \tau_{xy} \end{bmatrix}_n = [\bar{Q}]_n [\varepsilon]_n \tag{19}$$

For first ply failure determination, σ_x is set equal to the transverse strength of the 90° ply. Then it is possible to solve for N_x and determine the applied stress that causes first ply failure.

2. Young's Modulus Prediction

Using some of the results of the preceding section, it is possible to predict the Young's modulus of the composite laminate. Equation (15) provides a relation between the mid-plane strain of the laminate and the applied stress. Thus, for uni-axial tension, the Young's modulus can be determined from the first term of the $[A_1]$ matrix as follows

$$E_c = \frac{1}{(t)A_{1_{11}}} \tag{20}$$

where E_c is the Young's modulus of the composite and t is the thickness of the laminate.

Using the ply discount method, it is also possible to predict the value of Young's modulus after first ply failure.

The ply discount method assumes that after cracking, the 90° plies are unable to carry any of the load. This method is applied by setting $[\bar{Q}]$ for the 90° ply equal to zero in equations (7), (8), and (9). This results in a new $[A_1]$ matrix and by using equation (20), the Young's modulus after first ply failure can be found.

3. Crack Density Theoretical Model

The initiation of cracks and the multiplication of cracks to a saturation level are the important physical aspects of the transverse cracking process. In a cross-ply laminate under uni-axial loading, the transverse ply is a material of low failure strain placed between plies of a higher failure strain. In this situation, multiple transverse cracking occurs in the transverse ply. This section will outline a theoretical model proposed by Garrett and Bailey (1:162-163) to predict the transverse crack density in a cross-ply laminate.

Figure 2 shows the laminate layout used in the development of the theoretical crack density model. It is assumed that the transverse ply has a unique breaking strain, ε_{tu}, and strength σ_{tu}. When a stress is applied in a direction parallel to the longitudinal plies, the transverse ply will fail at a stress equal to σ_{tu}. At that point, the load that was being carried by the transverse ply will be transferred to the longitudinal plies. Matrix cracking can

occur in the transverse ply if sufficient stress is applied and the following inequality is satisfied:

$$\sigma_{lu} b \geq \sigma_{tu} d + \sigma_l' b \tag{21}$$

where σ_{lu} is the strength of the longitudinal plies and σ_l' is the stress on the longitudinal plies when the transverse ply fails. If the inequality is not satisfied, then the

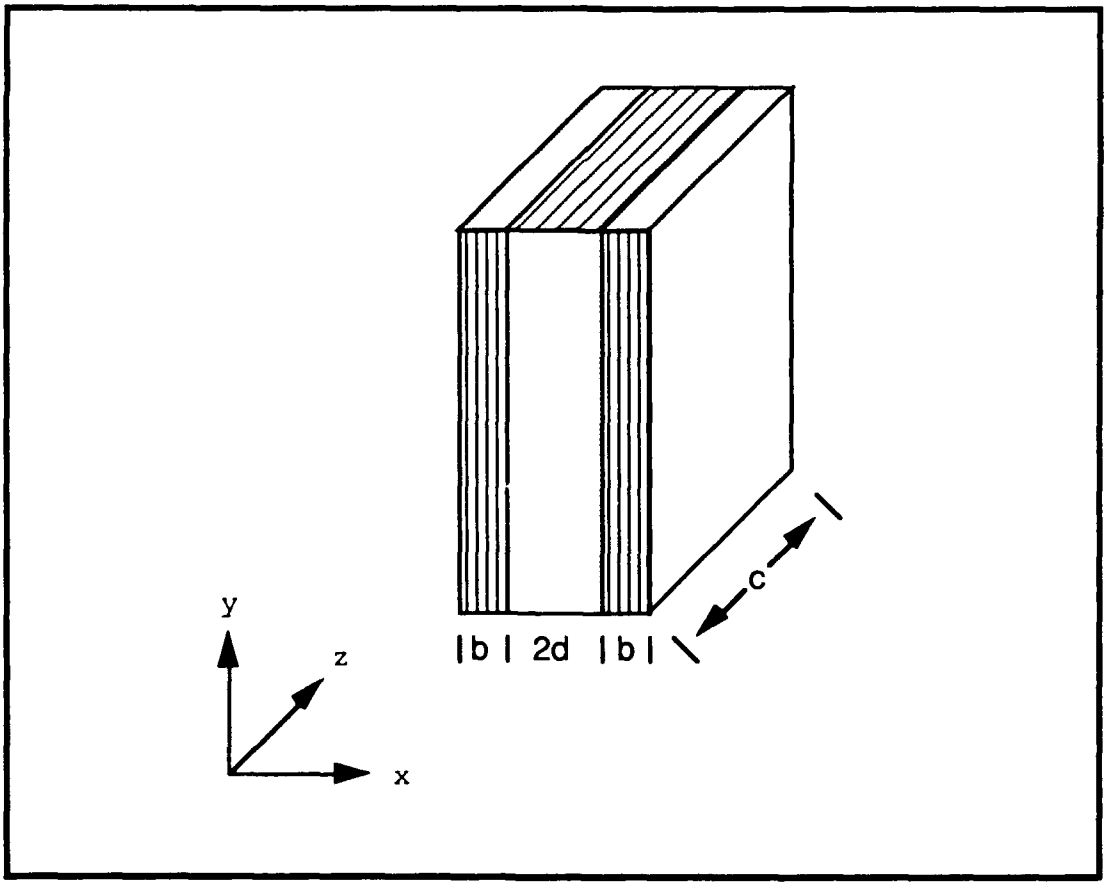

Figure 2. Specimen Model

longitudinal plies are unable to carry the extra load placed on them and failure will occur.

When multiple transverse cracking occurs, the equation governing the load transfer between the longitudinal and transverse plies is

$$\frac{dF}{dy} = 2c\tau_i \tag{22}$$

where dF is the load transferred from the two longitudinal plies in distance dy at an interface shear stress τ_i. The behavior of τ_i along the interface is of primary importance in determining the rate at which the load is transferred back into the transverse ply and hence the resulting crack spacing. If the interface between the plies is considered to be elastically bonded, τ_i will be a function of y.

After the first crack has occurred in the transverse ply at a strain ε_{tu}, an additional stress, $\Delta\sigma$, is placed on the longitudinal plies. This additional stress has its maximum value $\Delta\sigma_0$ in the plane of the crack and decays with distance y from the crack surface as some load is transferred back into the transverse ply. Assuming an even load distribution in the longitudinal plies gives

$$\Delta\sigma_0 = \sigma_a \cdot \frac{b + d}{b} - E_l\varepsilon_{tu} \tag{23}$$

where σ_a is the applied stress on the specimen and E_1 is the Young's modulus of the longitudinal ply. Through the use of a shear lag analysis for cross-ply laminates, Garrett and Bailey (1:162) found that

$$\Delta\sigma = \Delta\sigma_0 \exp(-\phi^{0.5} y) \tag{24}$$

where

$$\phi = \frac{E_c G_t}{E_1 E_t} \left[\frac{b + d}{bd^2} \right] \tag{25}$$

E_c is the Young's modulus of the laminate in the y-direction and G_t is the shear modulus of the transverse ply in the y-direction.

From a simple force balance

$$\tau_i = -b \frac{d\Delta\sigma}{dy} \tag{26}$$

and therefore the shear stress at the ply interface may be found by substituting equation (24) into equation (26) and differentiating, giving

$$\tau_i = b\Delta\sigma\phi^{0.5} \exp(-\phi^{0.5} y) \tag{27}$$

From equations (22) and (27) the load F that is transferred back into the transverse ply at a given distance s from the plane of the crack is

$$F = 2bc\Delta\sigma_0[1 - \exp(-\phi^{0.5}s)] \tag{28}$$

The first crack in the transverse ply occurs when the load carried by it is equal to $2\sigma_{tu}dc$. This load is then transferred onto the longitudinal plies. Another crack can only occur when the transverse ply is again loaded to $2\sigma_{tu}dc$ by shear load transfer. For another crack to occur, σ_a must be increased to such a value that s in equation (28) lies within the length from the first crack to the nearest end on the specimen for F equal to $2\sigma_{tu}dc$.

Garrett and Bailey assumed that the first crack occurs in the middle of the specimen and that each succeeding crack falls exactly in the middle of two previous cracks. Thus with a specimen of length s, the following cracking sequence is predicted.

(a) Initial crack at $\Delta\sigma_0 = \sigma_{tu}d/b$ and $\sigma_a = E_c\varepsilon_{tu}$.

(b) Second and third cracks occur simultaneously at the ends of the specimen when the applied stress is such that

$$\Delta\sigma_0 = \sigma_{tu}\frac{d}{b}[1 - \exp(-\phi^{0.5}s/2)]^{-1} \tag{29}$$

This result is obtained by substituting $s/2$ for s and $F = 2\sigma_{tu}dc$ in equation (28). At this point, the crack spacing is $s/2$.

(c) The next series of cracks will occur midway between the present cracks, as the shear stress will build up from both cracks but will be of different signs. If the crack spacing is denoted by t, the total shear stress between the two cracks will be

$$\tau = b\Delta\sigma_0\phi^{0.5}[\exp(-\phi^{0.5}y) - \exp(\phi^{0.5}(y - t))] \qquad (30)$$

and so

$$F = 2bc\Delta\sigma_0[1 + \exp(-\phi^{0.5}t) - 2\exp(-\phi^{0.5}t/2)] \qquad (31)$$

This result is obtained by substituting equation (30) into equation (22) and integrating between $t/2$ and 0. To determine the value of $\Delta\sigma_0$ when the cracks occur, $F = 2\sigma_{tu}dc$ is put into equation (31):

$$\Delta\sigma_0 = \sigma_{tu}\frac{d}{b}[1 + \exp(-\phi^{0.5}t) - 2\exp(-\phi^{0.5}t/2)]^{-1} \qquad (32)$$

At this stage of the cracking sequence $t = s/2$ so a crack spacing of $s/4$ will result when

$$\Delta\sigma_0 = \sigma_{tu}\frac{d}{b}[1 + \exp(-\phi^{0.5}s/2) - 2\exp(-\phi^{0.5}s/4)]^{-1} \qquad (33)$$

This cracking sequence will continue until the strength of the longitudinal plies is exceeded or debonding occurs if the shear stress in equation (27) exceeds the shear strength of the interface.

Application of this theory results in a stepped curve for crack spacing versus applied stress. The length of the steps in the curve increases as the overall applied stress increases. Therefore, at high applied stresses the crack spacing will remain unchanged for a large range of applied stresses and will approach a saturation spacing. In comparisons to experimental data, this theory has been shown to provide the proper trends in crack spacing but to considerably overestimate the saturation crack density.

Other models have been proposed for calculating the theoretical transverse cracking behavior of polymer composites, but they have their drawbacks. Laws and Dvorak (9:906-909) proposed using a probability density function for additional cracking that was proportional to the stress in the transverse ply. The disadvantage of this theory is that it results in an extremely complex integral that must be evaluated numerically. An energy method has been suggested by Wang and Crossman (10:76-83). While this theory does show some correlation to experimental data, it requires extensive finite element modeling. Thus, for reasons of simplicity, it was decided to proceed using Garrett and Bailey's theory and

at least be able to predict the data trends for crack spacing as a function of transverse ply thickness.

III. Experimental Procedure

This chapter will discuss sample preparation, test procedures, and data reduction.

A. Sample Preparation

This section will describe the material, discuss how the specimens were prepared for testing, and explain how the fiber volume fraction was obtained.

The ceramic composite used in this study, SiC/1723, was manufactured at the Wright Research and Development Center, Wright-Patterson AFB. The basic components of SiC/1723 are an aluminosilicate glass frit, a binder solution, and silicon carbide yarn. The glass frit consists of a 1723 Corning amorphous glass mixture which comes in the form of a finely ground powder. The R Hoplex Binder comes in the form of a liquid. The silicon carbide fibers are Nicalon yarn manufactured by the Nippon Carbon Company of Tokyo. For complete details on the manufacturing process, see Appendix A of Vozzola (11:52). Mr. Larry Zawada of the Wright Research and Development Center (12) provided the following data for unidirectional SiC/1723 composite:

Axial Modulus, E_1 = 20.3 msi
Transverse Modulus, E_2 = 12.76 msi
Shear Modulus, G_{12} = 6.38 ksi
Ultimate Strain for Transverse Ply, ε_{tu} = 217 $\mu\varepsilon$

The material was supplied in the form of four inch by four inch panels. Individual straight-sided specimens were cut using a Buehler Isomet low speed saw with a diamond blade. Special care was taken to minimize cutting edge damage. The nominal width of all the specimens was 0.25 in. Beveled end tabs made of 1/16 inch thick 0/90 glass/epoxy were bonded to the ends of the specimens for gripping during testing. The tabs were bonded using epoxy cement cured at 225°F for one hour. Figure 3 shows the specimen layout, and Table 1 provides the dimensions of each test specimen.

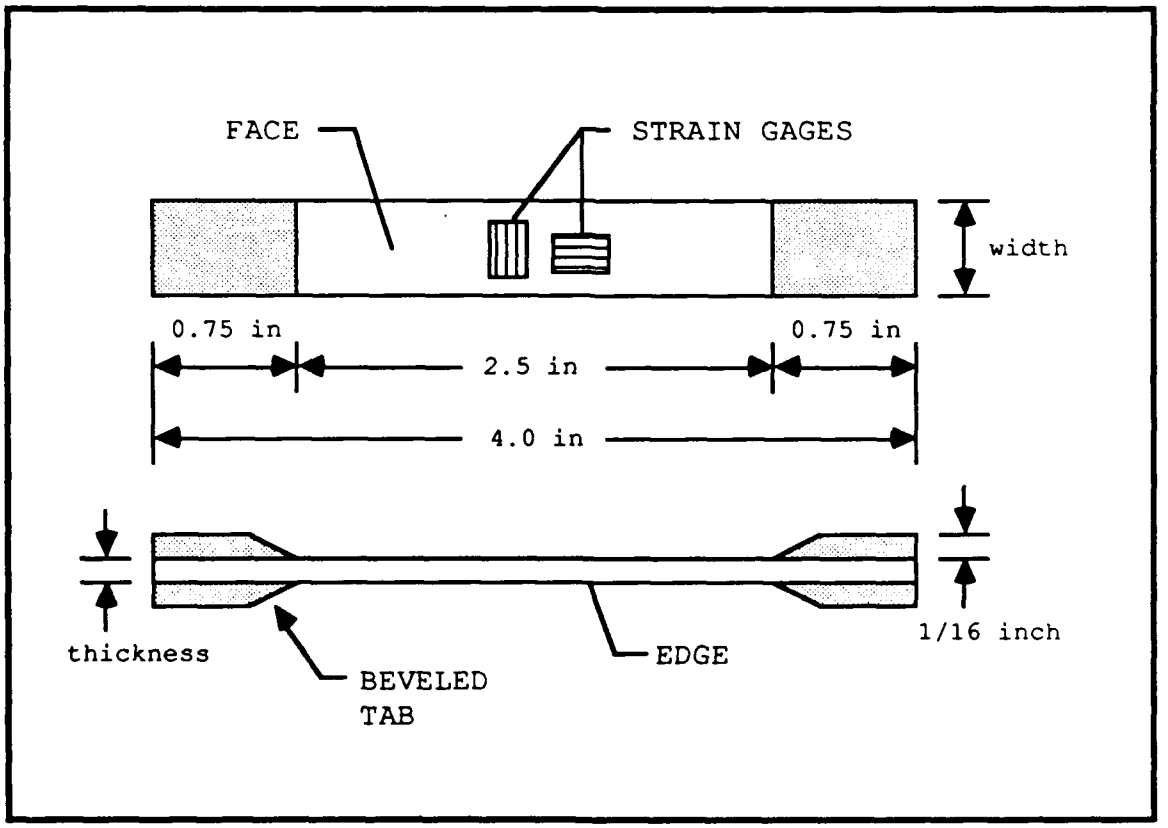

Figure 3. General Specimen Layout

Table 1
Specimen Dimensions

Specimen Number[1]	Width (in)	Thickness (in)	Cross-Sectional Area (in^2)
$0_3/90/0_3$			
90C16-01	0.248	0.070	0.0174
90C16-02	0.238	0.074	0.0178
90C16-03	0.249	0.076	0.0189
90C16-04	0.257	0.066	0.0170
90C16-05	0.254	0.065	0.0165
$0_3/90_2/0_3$			
90C17-03	0.241	0.078	0.0190
90C17-05	0.232	0.072	0.0168
90C17-06	0.241	0.073	0.0176
90C17-07	0.261	0.079	0.0207
90C17-08	0.257	0.081	0.0207
90C17-09	0.265	0.079	0.0209
$0_3/90_3/0_3$			
90C15-01	0.248	0.082	0.0203
90C15-02	0.256	0.082	0.0210
90C15-03	0.248	0.082	0.0204
90C15-04	0.248	0.079	0.0195
90C15-05	0.271	0.077	0.0209
$0/90/0_4/90/0$			
90C30-01	0.244	0.085	0.0207
90C30-02	0.248	0.085	0.0211
90C30-03	0.198	0.088	0.0174
90C30-04	0.181	0.087	0.0157

[1]The first 5 digits of the specimen number identify the lay-up

After tabbing, each specimen was polished on one edge to enhance microscopic imaging and replication for crack detection. A polishing fixture, as shown in Figure 4, was used to polish two specimens at a time. The specimens were first wet sanded on a polishing wheel with 600 and 800 grit aluminum oxide sandpaper. Then the specimens were polished on the wheel using 3.0, 1.0, and 0.3 micron alumina.

Next, two 120Ω strain gages (Micro Measurements type CEA-06-032UW-120) were attached to one side of each specimen.

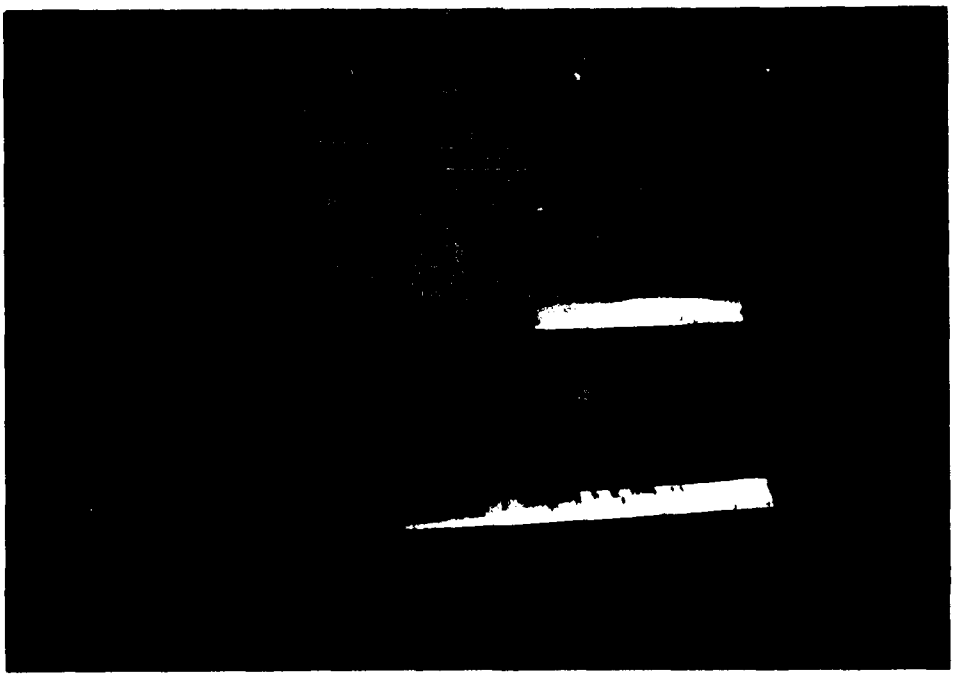

Figure 4. Polishing Fixture

One gage was applied in the axial load direction and one in the transverse direction, as shown in Figure 3.

The volume fiber fraction (V_f) was obtained by taking ten micrographs of the polished transverse plies at 400x, see Figure 5. The average fiber diameter in SiC/1723 is 4.92 x 10^{-4} in. (12). The number of fibers was counted in each micrograph and V_f was calculated using the following formula:

$$V_f = \frac{nA_f}{A_p} \tag{32}$$

where,

n = number of fibers in picture

A_f = Area of the fibers

A_p = Area of the picture

Then the ten volume fractions were averaged to give a composite fiber volume fraction, which was found to be 0.39.

B. Test Procedures

This section will discuss the test methodology, including replication and acoustic emission. All of the specimens were tested in tension on an Instron model 1011 testing machine at a cross-head speed of 0.01 in/minute. Small wedge grips were designed to hold the specimens while they were under test. The choice of wedge grips was important, as some early tests with other types of grips

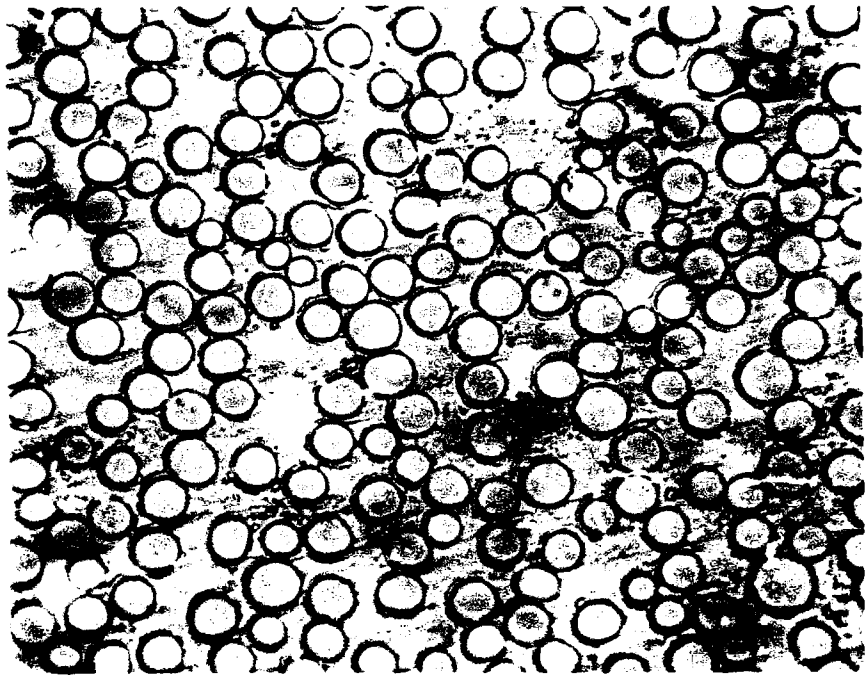

Figure 5. Sample Volume Fraction Calculation Picture (400x)

always resulted in tab area failures. Figure 6 shows the test set-up with a specimen installed.

Replication was used to monitor crack initiation and crack progression. The replication technique uses a cellulose-acetate film to record the surface topography of a material and yields much information on the development of damag along free edges. The film is applied to the desired surface, softened with acetone and allowed to set on the surface. The softened tape then flows into the underlying

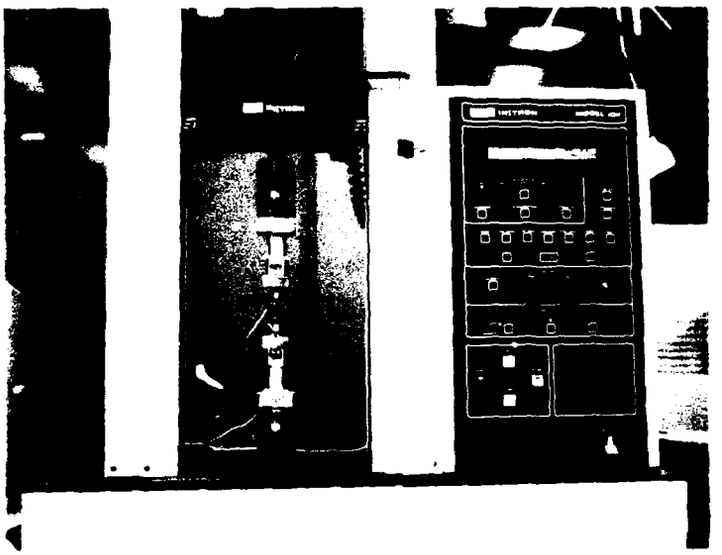

Figure 6. Instron Machine With Specimen Installed

surface and when set, creates an exact duplicate record of that surface.

The first two specimens of each lay-up were tested with an acoustic emission system in an attempt to pick up the noise of the initial transverse cracking. In subsequent tests, replications were concentrated near the stress levels where the acoustic emission indicated that cracking had occurred. In this manner it was possible to determine the stress level for crack initiation.

To determine the stress level for crack initiation, a replication was made at a stress level 1,000 psi below the level indicated by the acoustic emission. Then replications were made every 200 psi until a crack was detected. To monitor crack progression and crack density, replications were taken at intervals of approximately 4 ksi up to failure.

The signals from the strain gages were sent through strain gage amplifiers to a computer program. The computer program allowed continuous monitoring of transverse strain, axial strain, applied load, applied stress, Young's modulus and Poisson's ratio.

To record the transverse crack progression, micrographs were taken from the replications using an Olympus inverted metallurgical microscope with an attached Polaroid camera.

C. Data Reduction

As mentioned previously, a computer program was utilized to collect and reduce the data from the two strain gages. This program calculated Young's modulus and Poisson's ratio as the tests progressed. The stress and strain data from the data acquisition program were transferred directly to a graphics program to produce the stress-strain curves. The ultimate stress and ultimate strain values for each specimen were taken from the computer program.

The stress level for crack initiation was determined by examining a series of replications that were made near the

stress levels indicated by the acoustic emission. The crack density was obtained by counting the number or cracks in a replication and dividing by the length of the replication, which was typically one inch long. The crack spacing was found by inverting the crack density (i.e., a crack density of 4 cracks per inch is a crack spacing of 0.25 inches).

IV. Results and Discussion

This chapter contains the results and discussion of the experimental tests and comparisons of the test data to the theoretical models. The first part of the chapter will discuss some general problems related to the tested ceramic composite material and specimen preparation. The second section will discuss the crack initiation and progression in each lay-up separately. The third section will compare the performance of the four lay-ups and discuss some of their common cracking behavior. The fourth section will compare the test results to the theoretical models outlined in Chapter II. The final section will compare the experimental results to similar tests with glass/epoxy and graphite/epoxy systems.

A. Material Preparation

After polishing two of the specimens from the $0_3/90_3/0_3$ plate, it was discovered that several very thin cracks were present in the 90° plies. Through discussions with Mr. Larry Zawada of the Wright Research and Development Center (12) , it was determined that these cracks had most likely been caused when the plate was removed from its mold. One of these cracks is shown in Figure 7. Fink (13:31) encountered a similar problem in testing a ceramic composite and found

that these small pre-testing cracks had no effect on the performance of the composite. For this reason, it was decided to proceed with the testing of this plate. It should be noted that only two of the four specimens from this plate that were polished had these visible cracks prior to testing, and the data from the pre-cracked specimens was similar to the data from the uncracked specimens.

Another specimen preparation problem resulted from using a high-speed saw to cut two specimens from the $0_3/90_2/0_3$

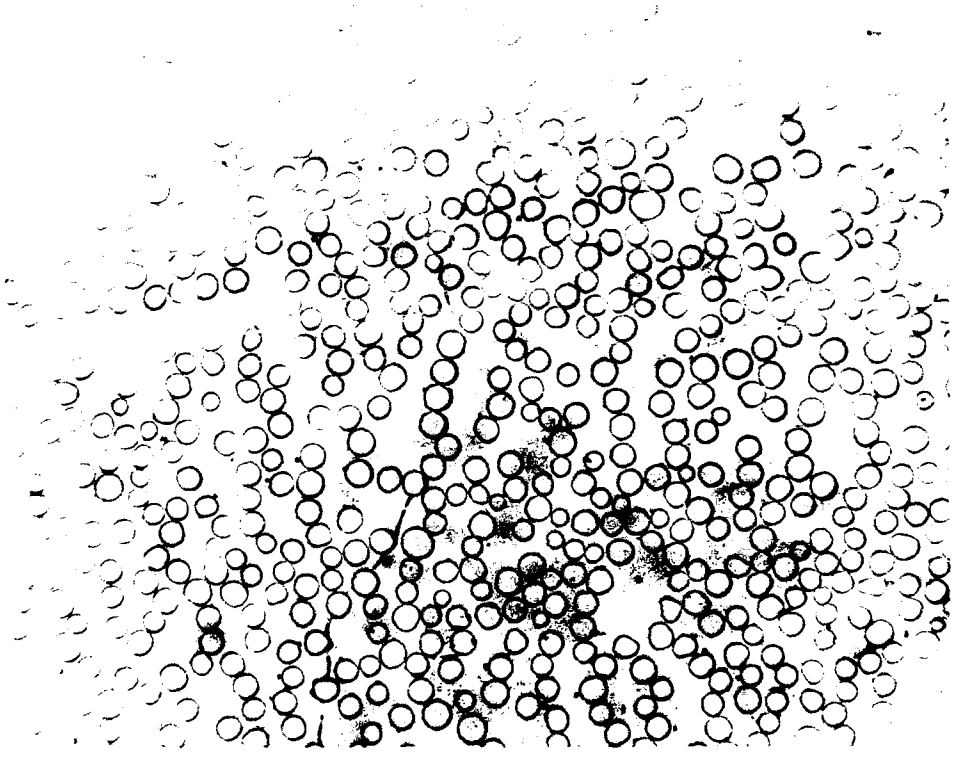

Figure 7. Crack in $0_3/90_3/0_3$ (Specimen 90C15-01) Prior to Testing

plate. Using the high-speed saw resulted in considerable edge damage which could not be polished out. These two specimens were not used, and the low-speed was used to cut all of the other specimens.

B. Crack Initiation and Crack Density

This section provides a brief summary of the test procedures and discusses the crack initiation and resulting crack density for each composite lay-up separately.

The test regime for each plate was broken into two distinct parts. The first set of tests was run to determine the transverse crack density and replications were taken at load intervals of approximately 4 ksi until failure. These tests were run using the acoustic emission system in an attempt to pick up the acoustic signal of the initial transverse cracking. The second set of tests was designed to determine the stress (and strain) level for crack initiation. To identify crack initiation, a replication was made at a stress level 1,000 psi below the level indicated by the acoustic emission. Then replications were made every 200 psi until a crack was detected.

The material properties determined from the testing are shown in Table 2. This table provides the material properties for each specimen and the average for each lay-up. Tabulated are the modulus of elasticity, Poisson's ratio, and the ultimate stress and strain. The subscript 1 denotes the

Table 2
Summary of Material Properties

Specimen Number	E_1 (msi)	ν_{12}	σ_1^{ult} (ksi)	ε_1^{ult} ($\mu\varepsilon$)
$0_3/90/0_3$				
90C16-01	16.848	0.18	40.625	2701
90C16-02	18.705	0.16	39.527	2061
90C16-03	18.850	0.20	41.190	2261
90C16-04	16.385	0.16	38.728	2354
90C16-05	18.995	0.21	41.770	4166
Average	17.957	0.18	40.368	2709
$0_3/90_2/0_3$				
90C17-03	17.189	0.25	43.753	3189
90C17-05	15.950	0.17	36.674	2571
90C17-06	15.515	0.17	28.468	1949
90C17-07	15.370	0.16	41.836	3060
90C17-08	15.370	0.17	43.131	3750
90C17-09	15.515	0.18	38.703	2762
Average	15.818	0.18	38.761	2880
$0_3/90_3/0_3$				
90C15-01	12.828	0.19	29.701	2557
90C15-02	14.500	0.22	32.341	2611
90C15-03	14.210	0.18	32.287	2955
90C15-04	11.727	0.21	30.682	2655
90C15-05	15.225	0.18	28.514	2295
Average	13.698	0.20	30.705	2615
$0/90/0_4/90/0$				
90C30-01	15.805	0.19	(1)	(1)
90C30-02	15.370	0.20	(1)	(1)
90C30-03	14.500	0.17	50.187	3934
90C30-04	15.515	NC	58.867	(2)
Average	15.300	0.19	54.527	3934

NC - Data not collected
(1) - Specimen did not break when loaded to machine's 1000 pound capacity
(2) - Axial strain exceeded the 5000 $\mu\varepsilon$ capacity of the strain gage amplifier setting

direction of the applied load while the subscript 2 is the direction perpendicular to the applied load. The superscript "ult" refers to the ultimate value.

1. $0_3/90/0_3$ Lay-up

A total of five specimens of this lay-up were tested. All broke in the gage length. A representative stress-strain curve is shown in Figure 8. The crack density of the first two specimens was studied. The transverse cracks usually formed at the $0^\circ/90^\circ$ ply interface and progressed straight through the 90° ply, perpendicular to the applied load. Figure 9 shows an early transverse crack in specimen 90C16-04. As can be seen from the micrograph, the crack is totally constrained by the 0° plies. As the applied load was increased more transverse cracks formed, evenly spaced along the length of the 90° ply. Figure 10 shows three evenly spaced transverse cracks. At this point, all of the damage was limited to the 90° ply as the 0° plies showed no cracking. As the applied load was further increased longitudinal cracks began to form, joining the transverse cracks together. This phenomenon can be seen in Figure 11. Reifsnider et al observed this same longitudinal cracking behavior in graphite/epoxy (6:20-22). Increasing the load even more resulted in an increase in the number of transverse cracks up to a point. Once a certain stress level was reached, the transverse ply became "saturated" and no new cracks developed. This result was expected based on the discussion

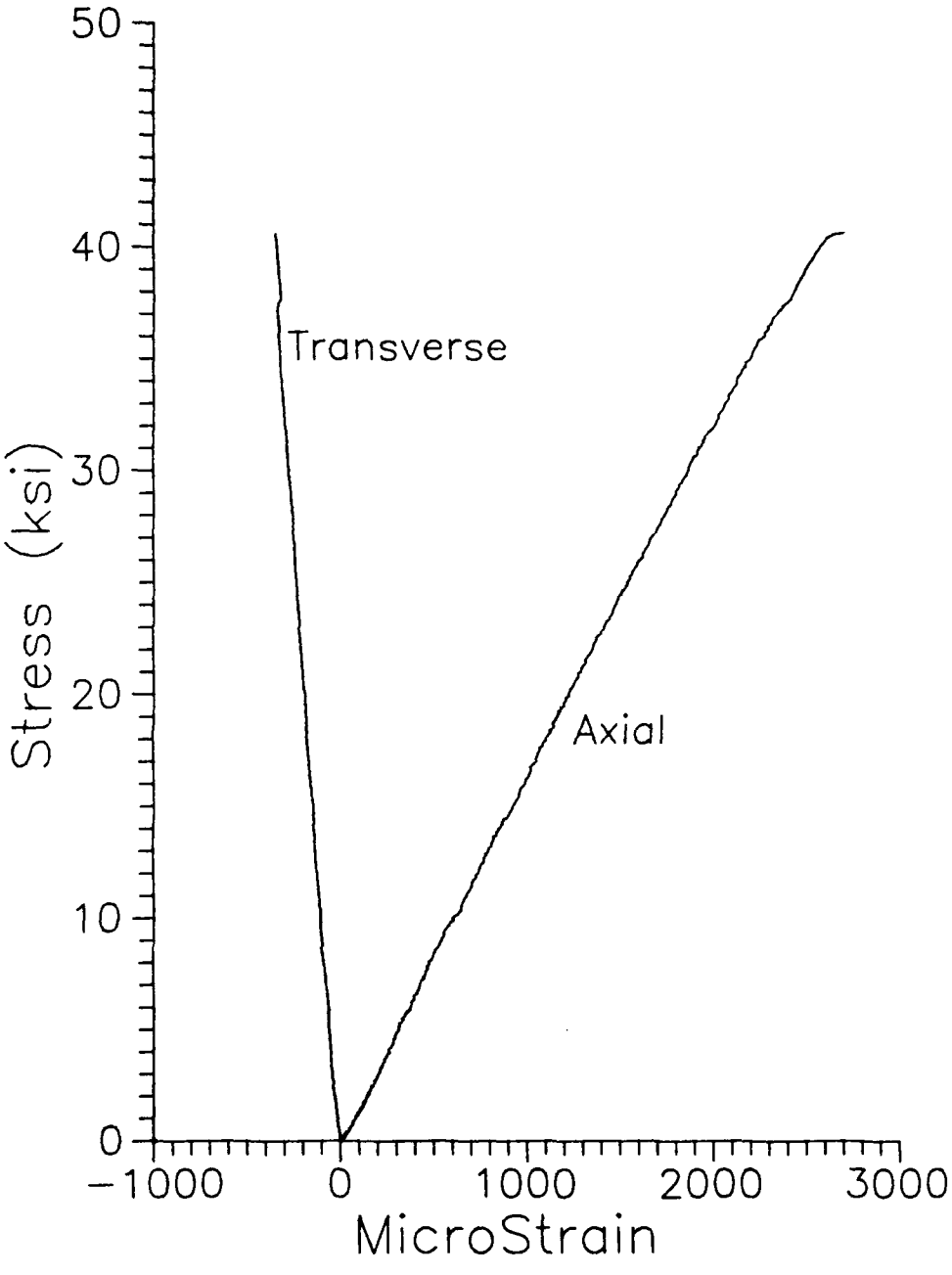

Figure 8. Stress-Strain Curve for $0_3/90/0_3$ (Specimen 90C16-01)

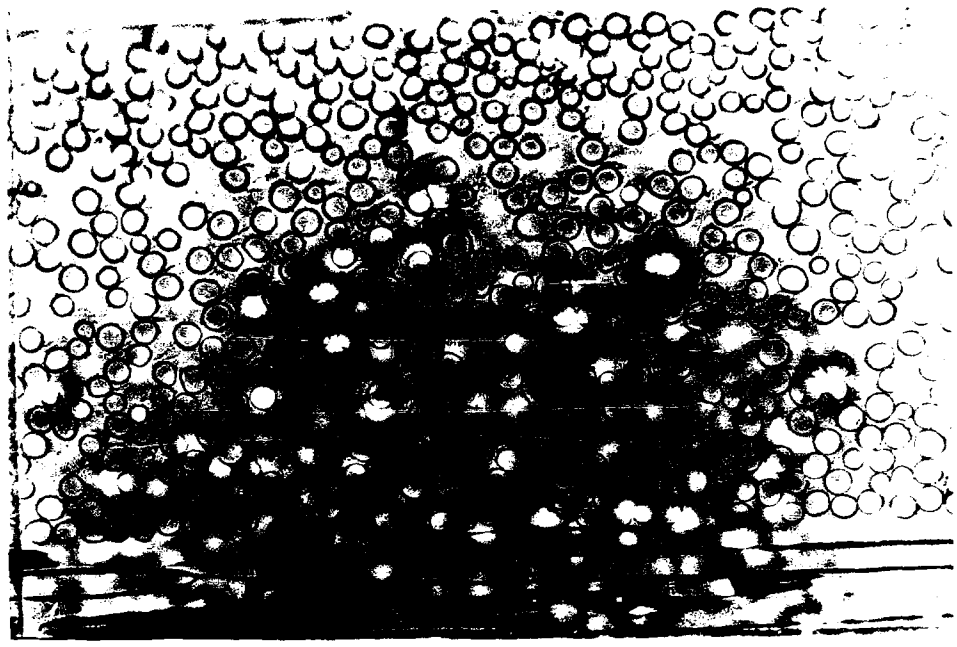

Figure 9. Transverse Crack in $0_3/90/0_3$ (Specimen 90C16-04) at 4.78 ksi (200x)

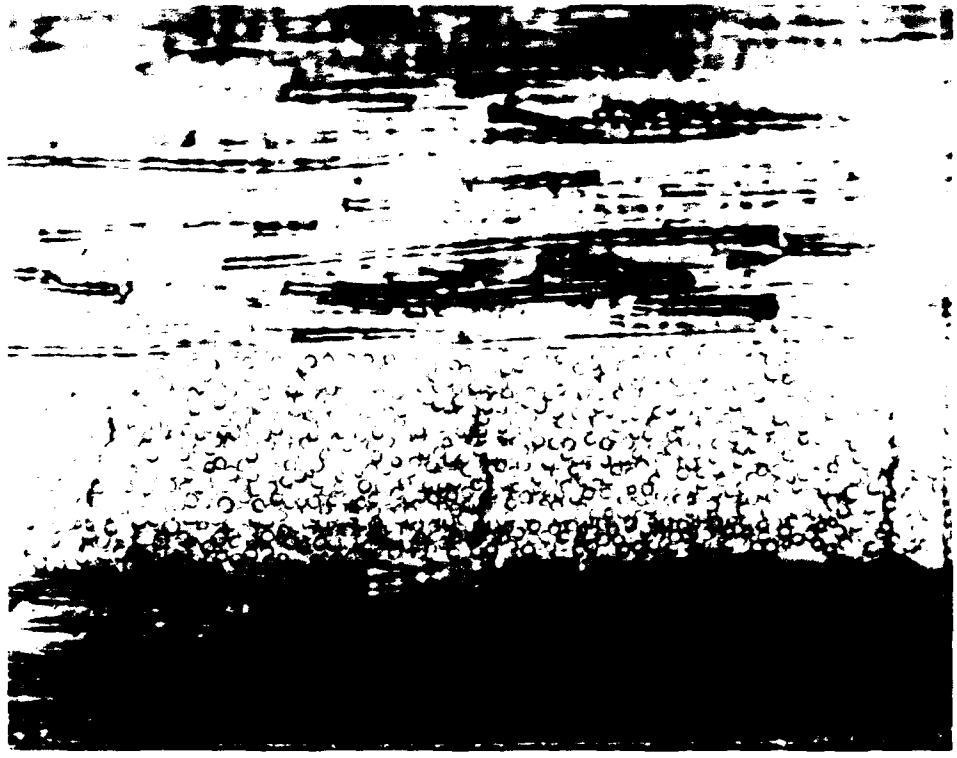

Figure 10. Evenly Spaced Cracks in $0_3/90/0_3$ at 5.28 ksi (100x)

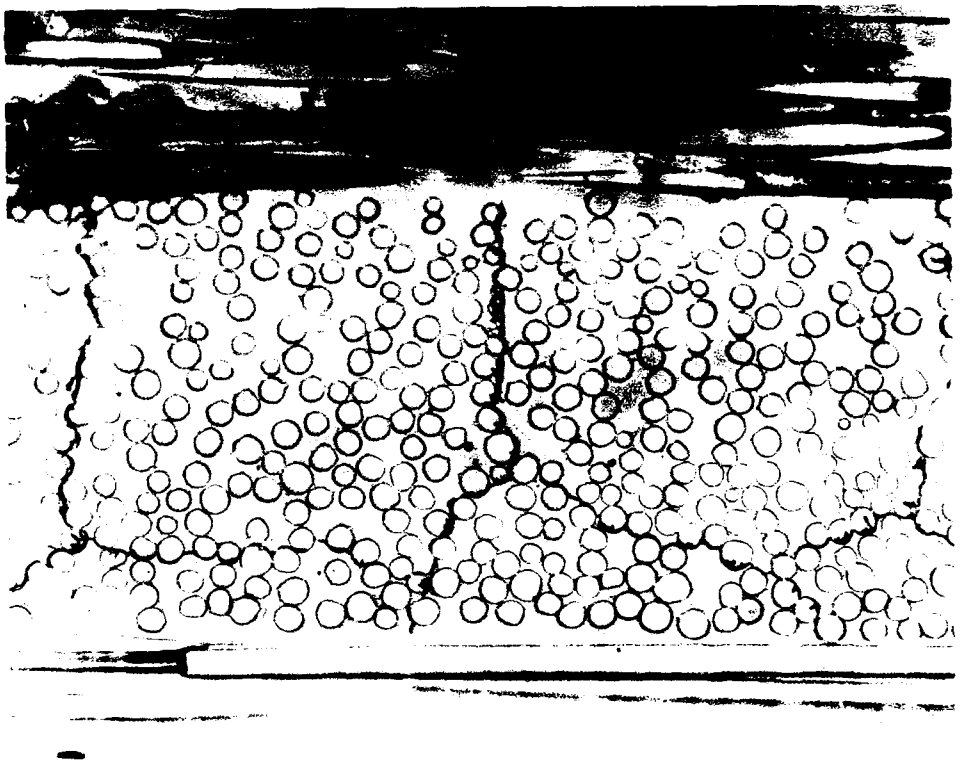

Figure 11. Longitudinal Cracks in $0_3/90/0_3$ at 10.081 ksi (200x)

in Chapter II. Table 3 presents the transverse crack spacing as a function of stress and strain for the two specimens studied, and the data are plotted in Figure 12. As can be seen from the table and the graph, the crack spacing reached a saturation spacing of between 0.0125 in and 0.0135 in.

Making use of the acoustic emission data from the tests on the first two specimens, the next task was to find the stress level that caused the first crack. This was done by concentrating replications near the stress level that was indicated by the acoustic emission. The first replication was made at a stress level 1,000 psi below the level at which the first acoustic emission signal was detected. Then replications were made every 200 psi until a crack was detected. Two specimens were tested in this manner. Following this procedure, the average stress and strain for the initial crack were found to be 5.010 ksi and 331 $\mu\varepsilon$, respectively. Figure 13 is a micrograph of the first crack in specimen 90C16-03.

Table 3
Stress, Strain and Crack Spacing for $0_3/90/0_3$ Lay-up

Specimen	Stress (ksi)	Strain (%)	Crack Spacing (in)
90C16-01	5.796	0.0354	0.0270
	10.100	0.0611	0.0181
	14.433	0.0874	0.0165
	20.144	0.1231	0.0143
	25.939	0.1602	0.0137
	31.707	0.1973	0.0136
	37.474	0.2388	0.0135
90C16-02	8.525	0.0466	0.1355
	11.303	0.0635	0.0244
	15.565	0.0879	0.0179
	19.800	0.1131	0.0160
	23.980	0.1380	0.0147
	29.645	0.1717	0.0132
	35.283	0.1973	0.0130
	39.518	0.2061	0.0125

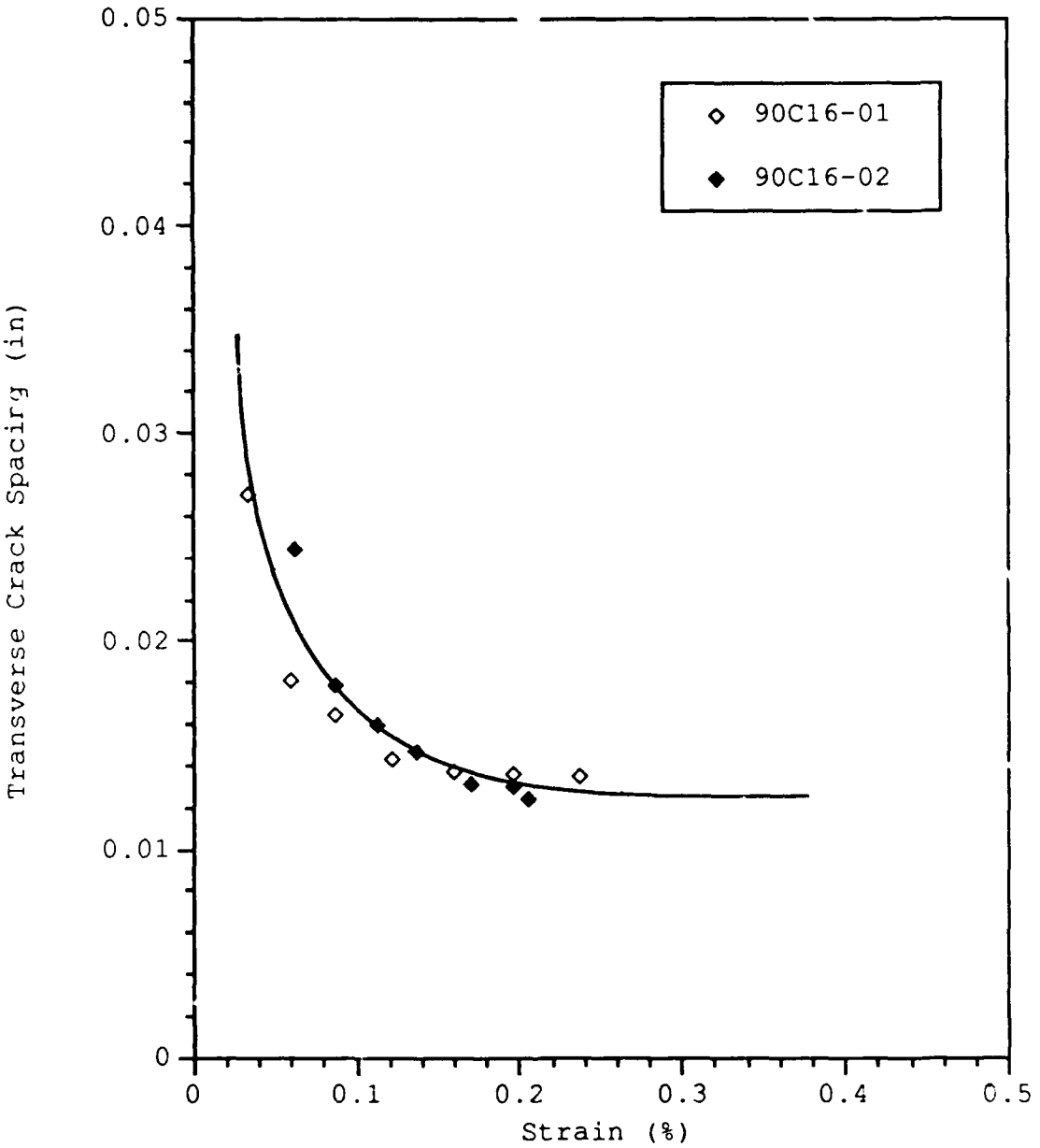

Figure 12. Crack Spacing as a Function of Strain for $0_3/90/0_3$

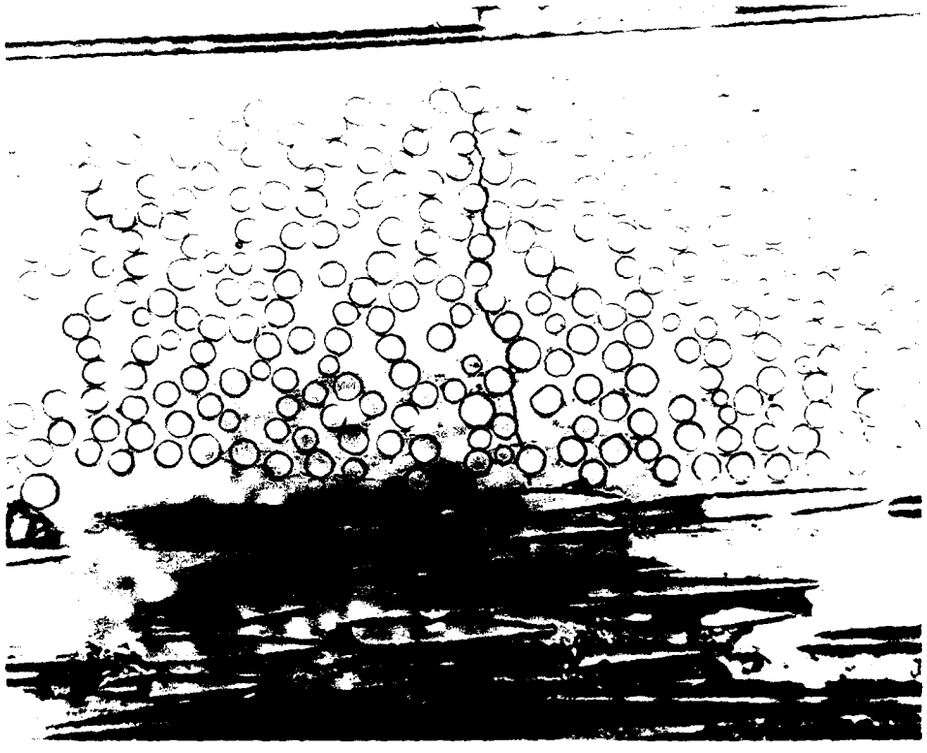

Figure 13. Initial Crack in $0_3/90/0_3$ at 5.058 ksi (200x)

2. $0_3/90_2/0_3$ Lay-up

A total of six specimens of this lay-up were tested. All broke in the gage length. A representative stress-strain curve is shown in Figure 14. The crack density of the first three specimens was studied. Once again, the transverse cracks usually formed at the $0^\circ/90^\circ$ ply interface and progressed straight through the 90° ply, perpendicular to the applied load. As with the $0_3/90/0_3$ lay-up, the transverse cracks developed with remarkably even spacing, followed by longitudinal cracks connecting the transverse cracks. The longitudinal cracks were seen in all of the specimens, always developing after the majority of the transverse cracks had formed. Figure 15 shows two transverse cracks connected by a longitudinal crack. A saturation crack spacing was also noted for this lay-up. Table 4 presents the transverse crack spacing as a function of stress and strain for the three specimens studied, and the data are plotted in Figure 16. As can be seen from the table and the graph, the crack spacing reached a saturation spacing of between 0.0209 in and 0.0228 in.

The average stress and strain for the initial crack were determined using a procedure similar to the one that was outlined for the $0_3/90/0_3$ lay-up. In this manner, the average stress and strain for crack initiation were found to be 4.800 ksi and 277 $\mu\varepsilon$, respectively. Figure 17 is a micrograph of the first crack in specimen 90C17-06 and shows that the

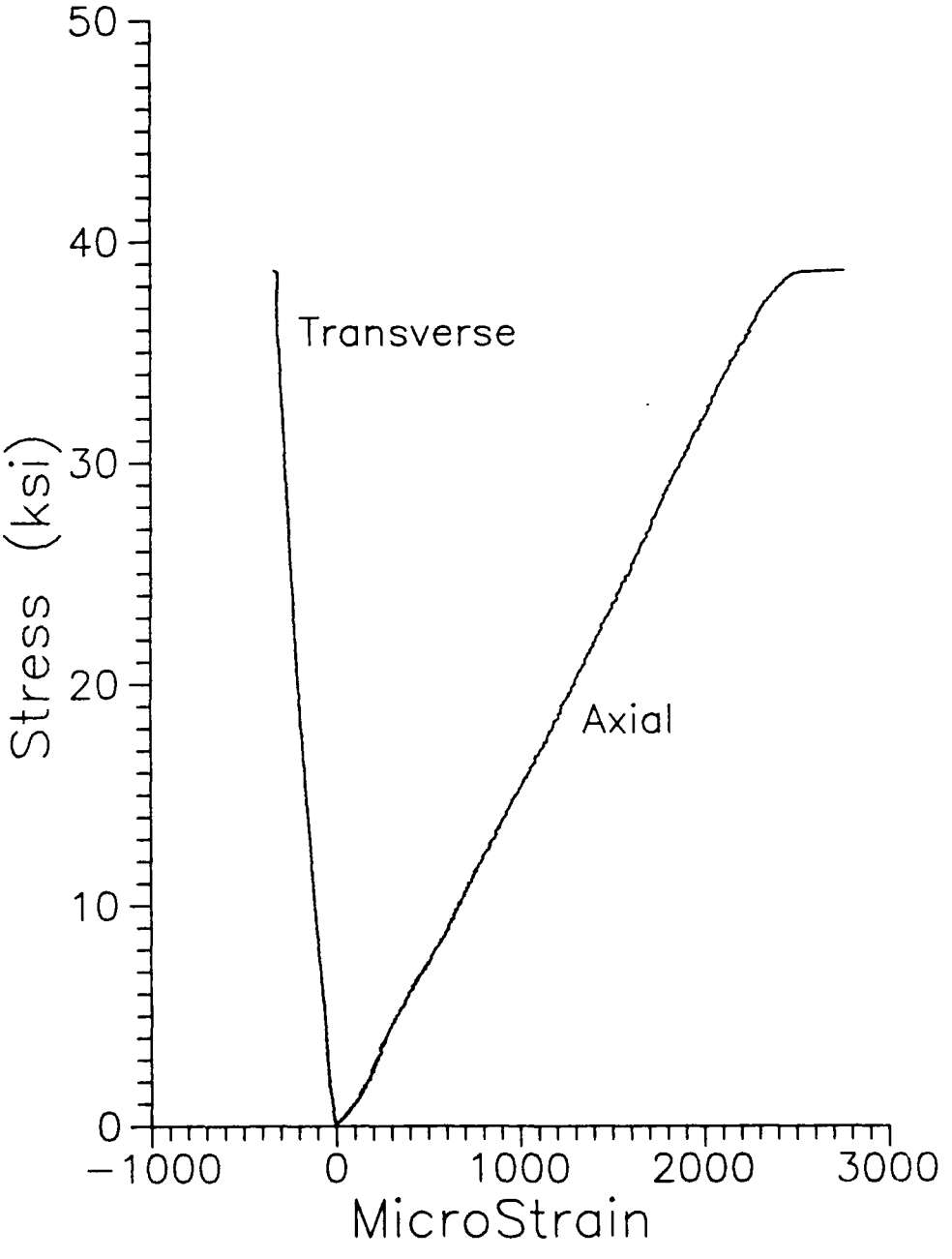

Figure 14. Stress-Strain Curve for $0_3/90_2/0_3$ (Specimen 90C17-09)

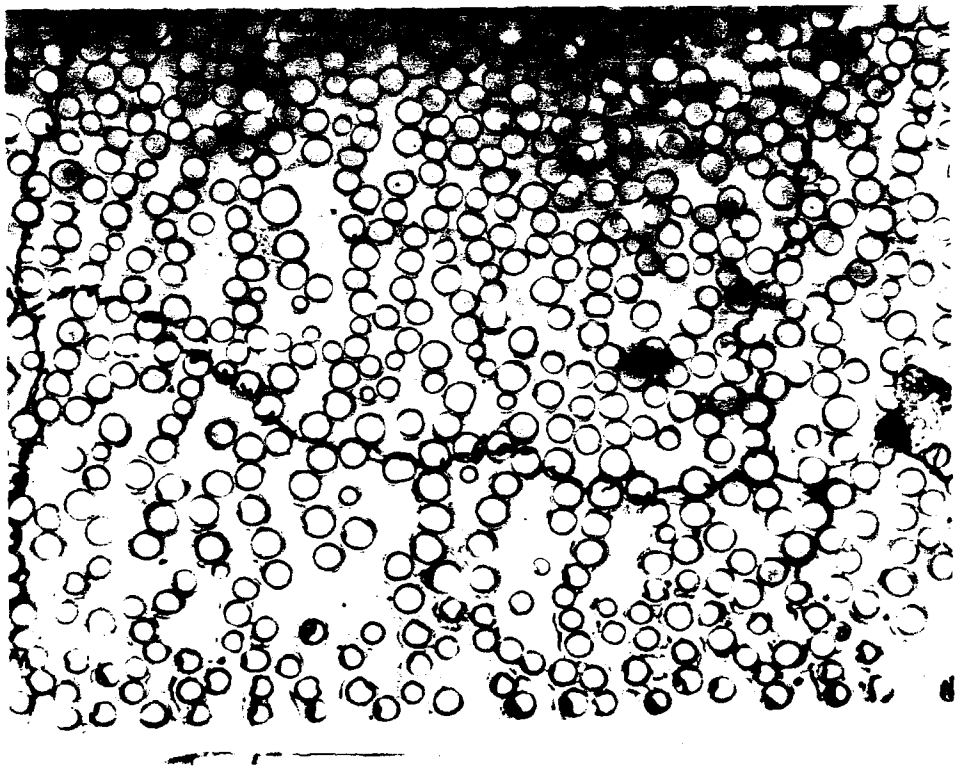

Figure 15. Transverse Cracks Connected by Longitudinal Crack in $0_3/90_2/0_3$ at 24.11 ksi (200x)

Table 4
Stress, Strain and Crack Spacing for $0_3/90_2/0_3$ Lay-up

Specimen	Stress (ksi)	Strain (%)	Crack Spacing (in)
90C17-03	5.319	0.0254	0.0470
	10.639	0.0598	0.0341
	15.959	0.0977	0.0290
	21.279	0.1321	0.0242
	26.599	0.1675	0.0232
	31.918	0.2083	0.0230
	37.238	0.2508	0.0230
	42.026	0.2962	0.0225
90C17-05	5.358	0.0332	0.0794
	7.025	0.0459	0.0446
	8.930	0.0586	0.0324
	13.395	0.0930	0.0272
	19.408	0.1331	0.0232
	24.112	0.1656	0.0214
	28.279	0.1924	0.0212
	32.625	0.2247	0.0209
90C17-06	4.555	0.0215	0.0703
	6.775	0.0383	0.0435
	11.387	0.0733	0.0362
	17.081	0.1121	0.0230
	22.774	0.1546	0.0228

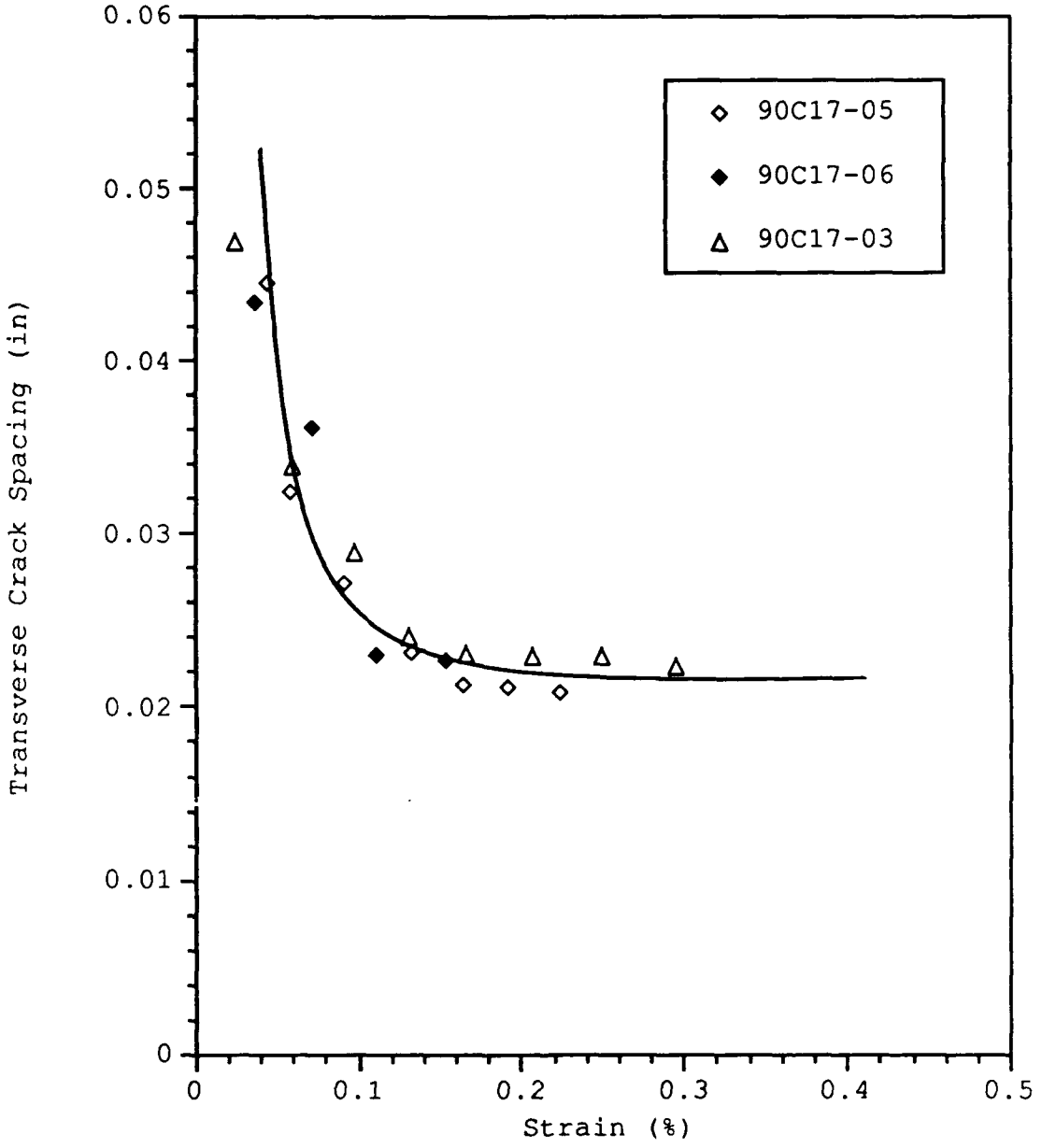

Figure 16. Crack Spacing as a Function of Strain for $0_3/90_2/0_3$

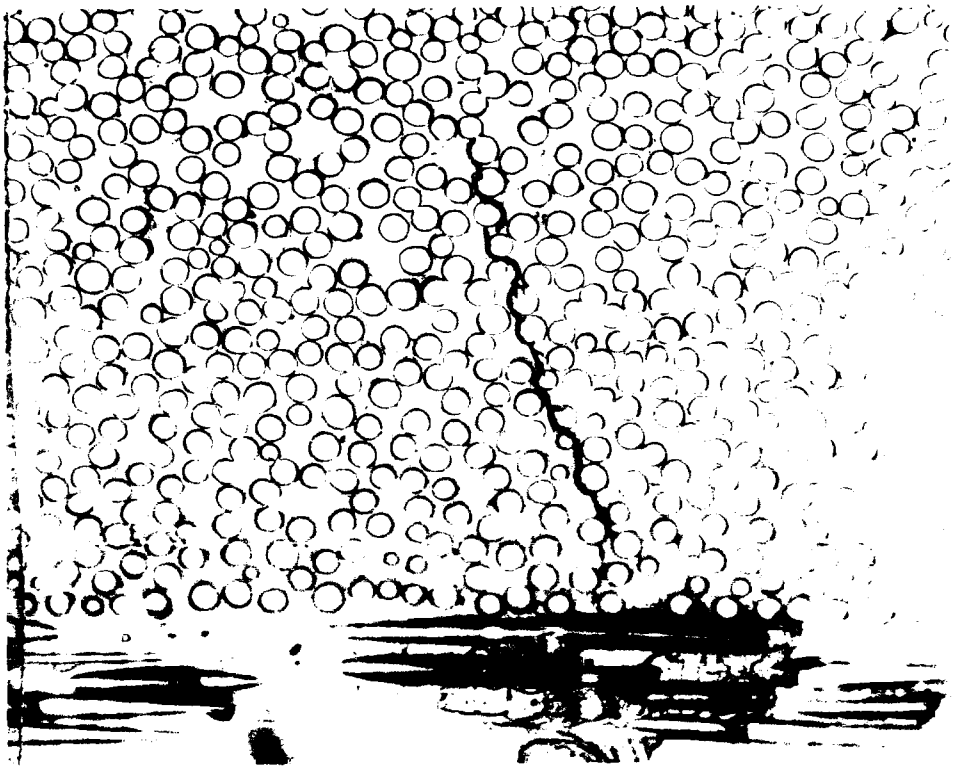

Figure 17. Initial Crack in $0_3/90_2/0_3$ at 4.555 ksi (200x)

transverse crack did develop near the $0^\circ/90^\circ$ ply interface and progressed through the 90° ply in a direction relatively perpendicular to the load.

3. $0_3/90_3/0_3$ Lay-up

A total of five specimens of this lay-up were tested. A representative stress-strain curve is shown in Figure 18. The crack density of the first three specimens was studied. As with the two previous lay-ups the transverse cracks usually developed at the $0^\circ/90^\circ$ ply interface and progressed through the 90° ply relatively perpendicular to the direction

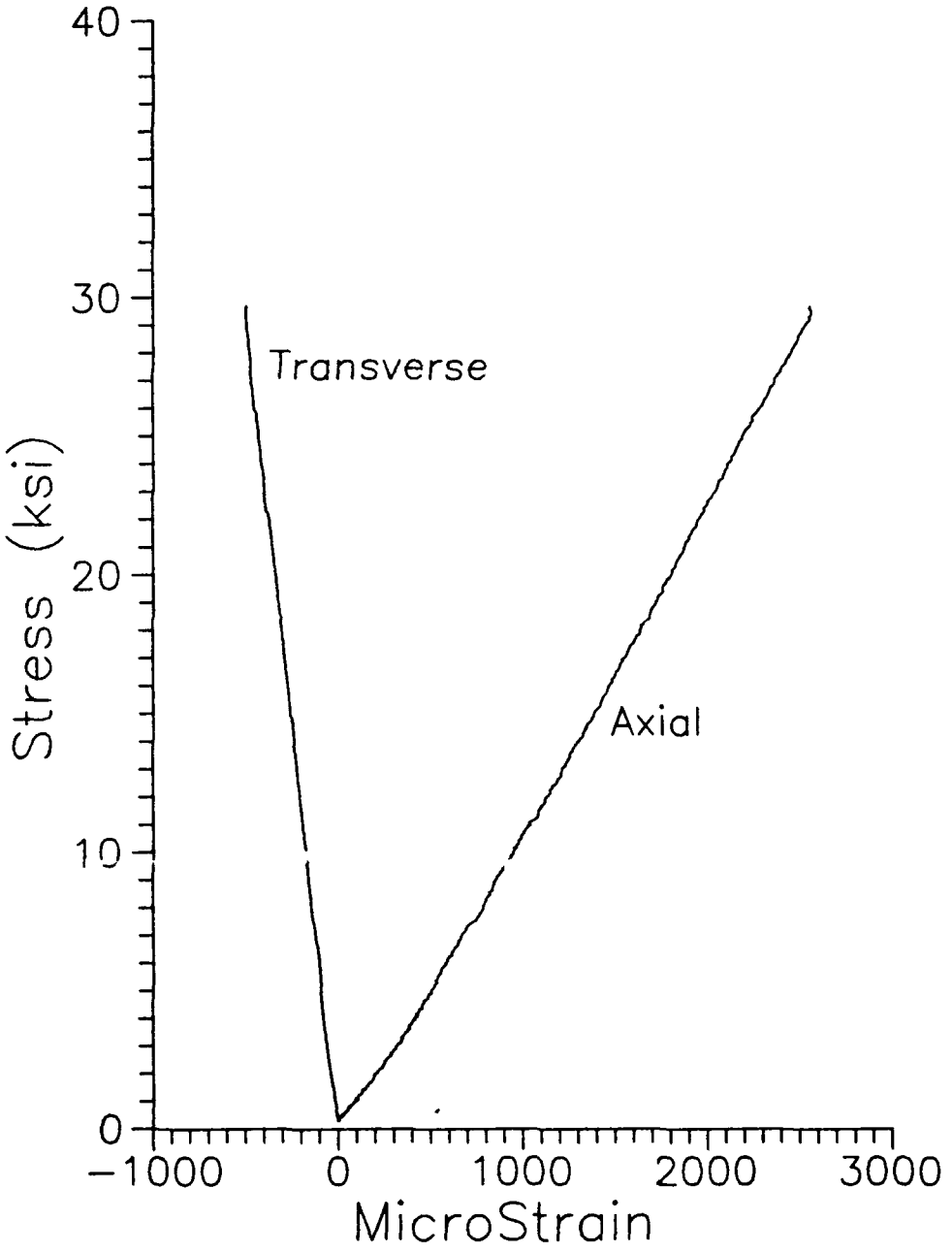

Figure 18. Stress-Strain Curve for $0_3/90_3/0_3$ (Specimen 90C15-01)

of the applied load. The transverse cracks again developed with even spacing, followed by the longitudinal cracks as shown in Figure 19. In the two previous lay-ups, the transverse cracking was constrained by the 0° plies, with the cracks travelling only one or two fiber diameters into the 0° plies. However, that was not the case for this lay-up. At low stress the 0° plies did constrain the transverse cracks. As the stress level was increased above 10 ksi, some of the transverse cracks penetrated the 0° plies and began to travel

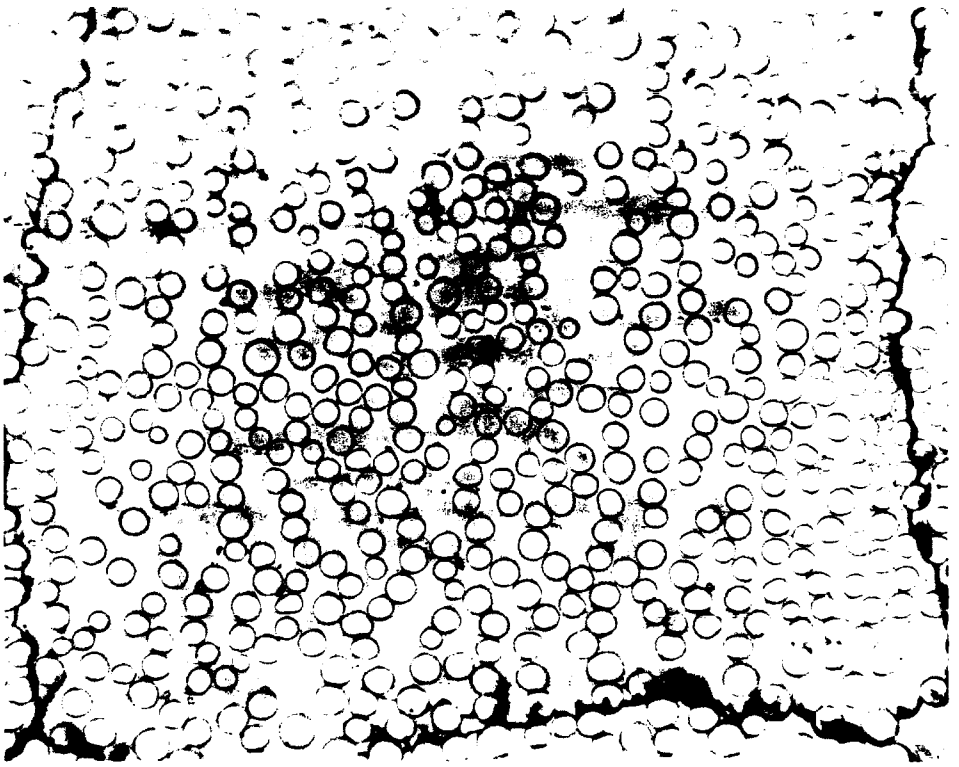

Figure 19. Transverse Cracks Connected by Longitudinal Crack in $0_3/90_3/0_3$ at 14.80 ksi (200x)

in the longitudinal direction. This can be seen in Figure 20. It is believed that these cracks, if sufficient in number, could cause delamination in the $0^{\circ}/90^{\circ}$ ply interface. Three of the five specimens tested did show some delamination at failure. This area clearly warrants further investigation.

Because of the cracks that were present in two of the specimens before testing (90C15-01 and -02), a special procedure was developed to track the crack spacing in those specimens. The specimens were loaded to a very low stress

Figure 20. Transverse Crack Penetrating 0° Ply in $0_3/90_3/0_3$ (200x)

(approximately 1 ksi) and a replication was made. This was done so that all of the manufacturing cracks would open and be visible in the replication. In this manner, a pre-testing crack density was found. The pre-testing crack density was then subtracted from the crack densities found at the higher stress levels. It was felt that following this procedure would result in the true crack density and hence the true transverse crack spacing. Table 5 presents the transverse crack spacing as a function of stress and strain for the three specimens studied. Figure 21 shows a graph of the transverse crack spacing versus the percent strain. As can be seen from the table and the graph, the crack spacing reached a saturation spacing of between 0.0330 in and 0.0351 in.

The average stress and strain for the initial crack in the $0_3/90_3/0_3$ lay-up were found to be 4.072 ksi and 273 $\mu\varepsilon$, respectively. Figure 22 is a micrograph of the first crack in specimen 90C15-03.

4. $0/90/0_4/90/0$ Lay-up

As discussed in Chapter I, this lay-up was chosen to study the effect of separating the 90° plies on crack initiation and crack density. The crack density and the stress for crack initiation were found for each of the 90° plies in the first two tested specimens of this lay-up. The third and fourth specimens were used only to obtain material properties (modulus of elasticity, ultimate stress,

Table 5
Stress, Strain and Crack Spacing for $0_3/90_3/0_3$ Lay-up

Specimen	Stress (ksi)	Strain (%)	Crack Spacing (in)
90C15-01	4.917	0.0503	0.2680
	11.064	0.1031	0.0413
	14.801	0.1370	0.0371
	18.440	0.1680	0.0351
	22.177	0.1968	0.0332
	25.865	0.2264	0.0330
90C15-02	4.049	0.0271	0.6410
	5.907	0.0381	0.1264
	9.527	0.0645	0.1238
	16.673	0.1221	0.0394
	20.246	0.1507	0.0356
	23.819	0.1780	0.0355
	27.487	0.2076	0.0351
90C15-04	2.564	0.0225	0.0800
	5.128	0.0437	0.0500
	8.975	0.0767	0.0422
	12.821	0.1079	0.0391
	16.667	0.1421	0.0356
	20.513	0.1744	0.0350
	24.411	0.2078	0.0339
	29.232	0.2508	0.0338

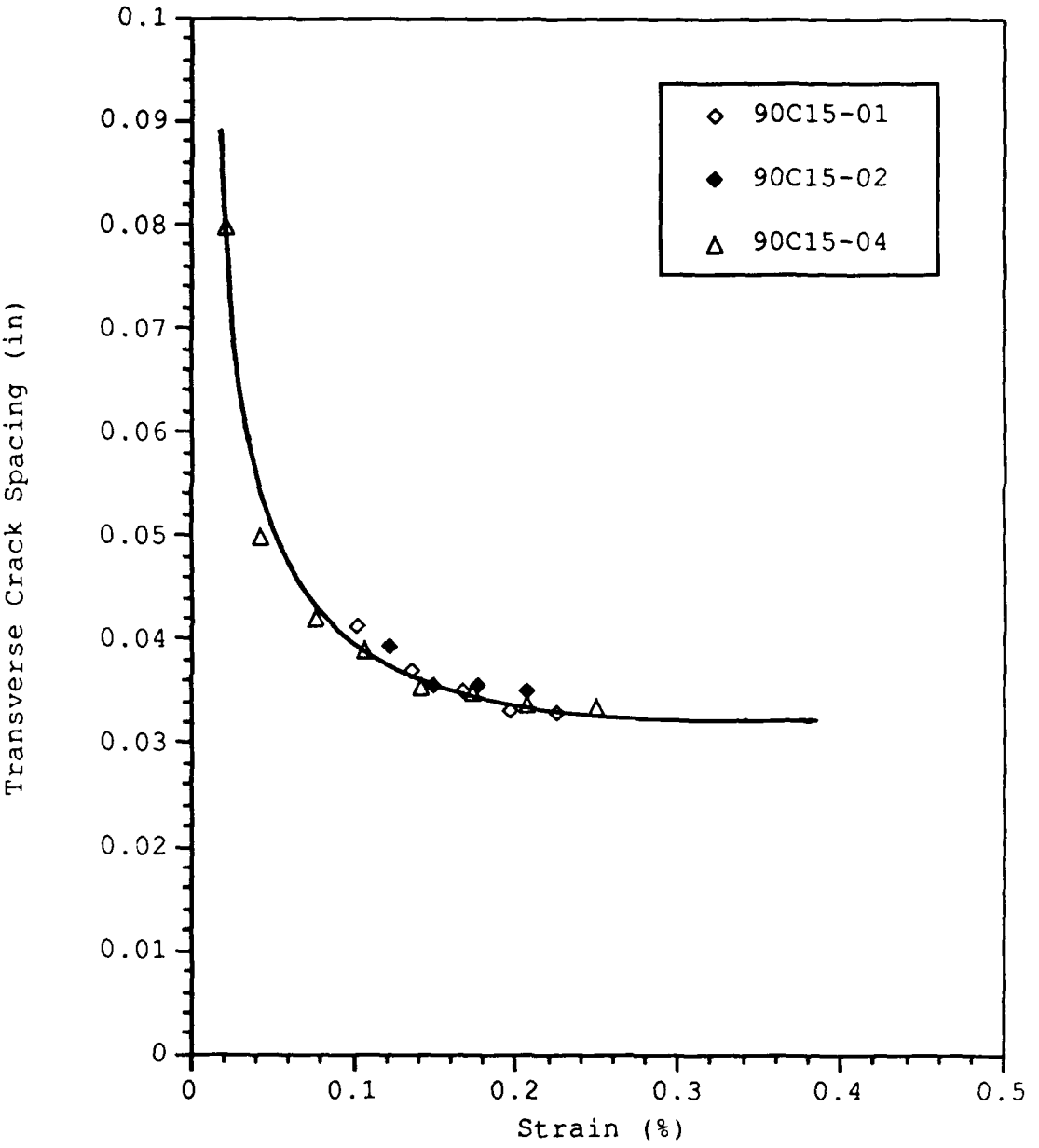

Figure 21. Crack Spacing as a Function of Strain for $0_3/90_3/0_3$

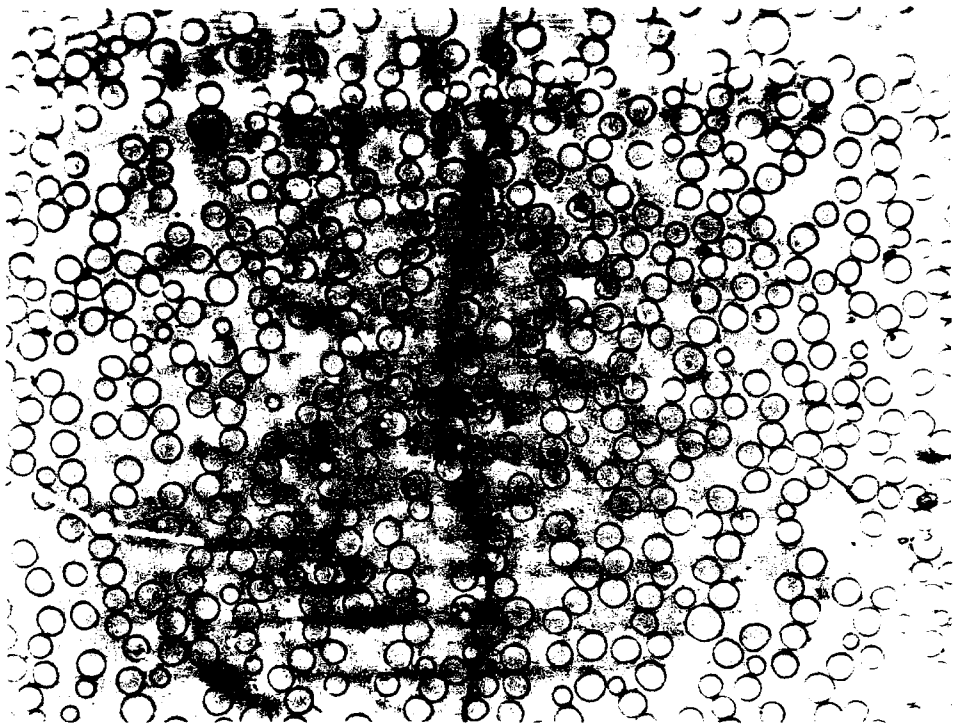

Figure 22. Initial Crack in $0_3/90_3/0_3$ at 3.92 ksi (200x)

Poisson's ratio, etc). A typical stress-strain curve is shown in Figure 23. It should be pointed out at this time that the fibers for the first three lay-ups ($0_3/90/0_3$, $0_3/90_2/0_3$ and $0_3/90_3/0_3$) all came from the same spool, but the fibers for the fourth lay-up ($0/90/0_4/90/0$) came from a different spool. This fact is most likely responsible for the $0/90/0_4/90/0$ lay-up being so much stronger than the other lay-ups.

Transverse cracks developed in this lay-up in a manner similar to the preceding lay-ups. Figure 24 shows a transverse crack in one of the 90° plies. Note that the crack formed in a matrix-rich region near the $0^\circ/90^\circ$ ply

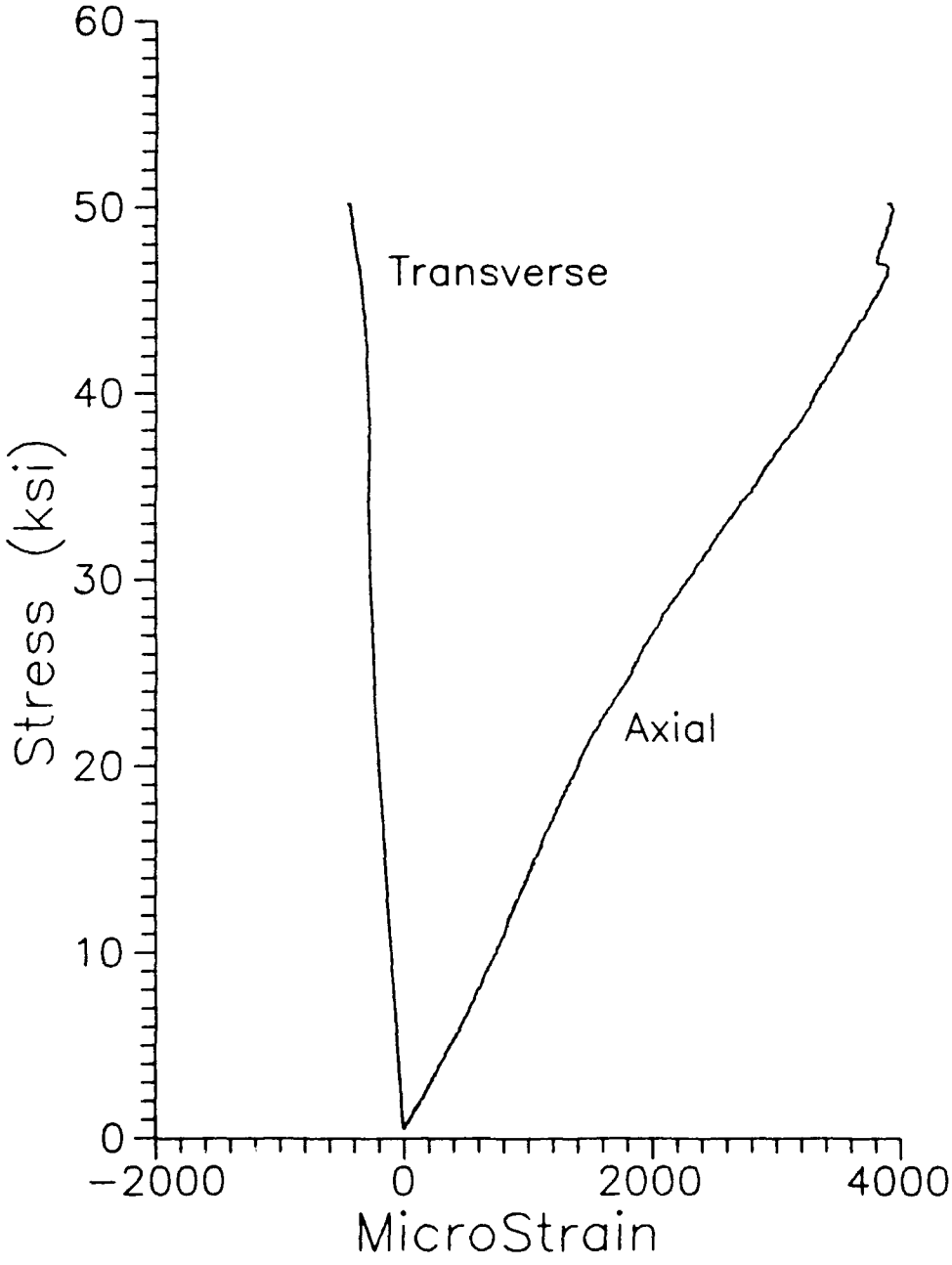

Figure 23. Stress-Strain Curve for $0/90/0_4/90/0$ (Specimen 90C30-03)

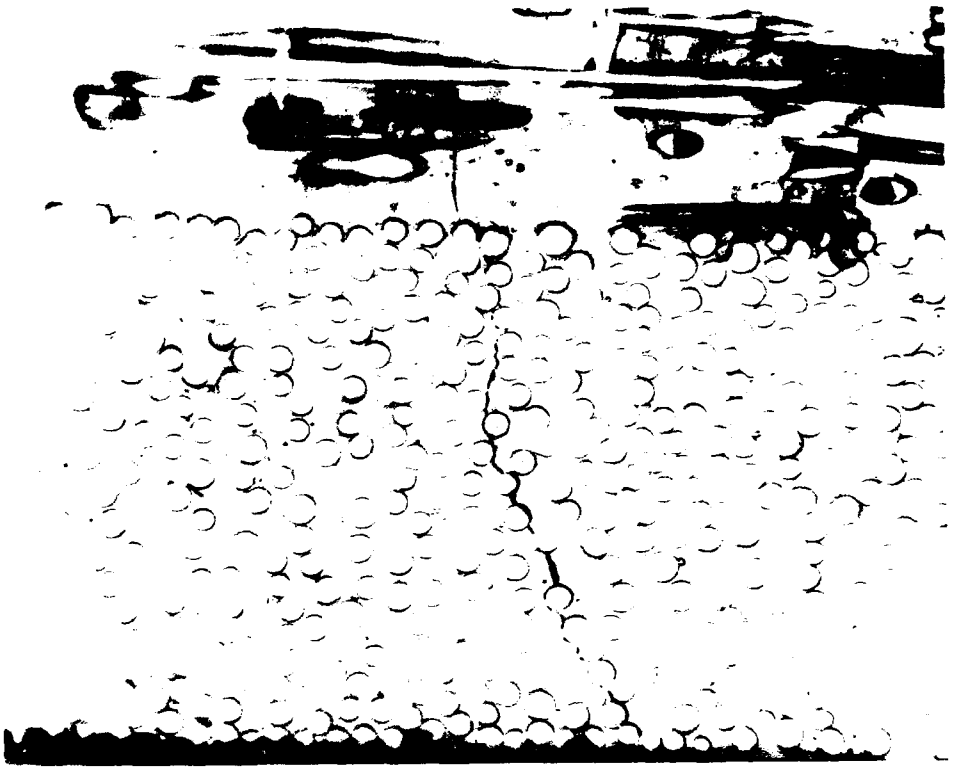

Figure 24. Transverse Crack in $0/90/0_4/90/0$ at 17.22 ksi (200x)

interface. Some localized matrix cracking in the 0° ply can also be seen at the top of this picture. Generally, the transverse cracks began to form in each individual 90° ply at about the same stress level. Longitudinal cracking was not as prevalent in this lay-up as it was in the first three lay-ups. When longitudinal cracking did appear, it was in relatively short lengths. Reifsnider et al also saw this phenomenon in distributed 90° plies (6:40). The transverse crack spacing in each of the 90° plies approached the same

saturation spacing. Table 6 presents the transverse crack spacing as a function of stress and strain for each of the 90° plies in the two specimens studied. The transverse crack spacing is graphed versus the percent strain in Figure 25. Although some scatter can be seen in the initial portions of the curve, the crack spacing of all the 90° plies did reach approximately the same saturation spacing. The saturation spacing for all of the 90° plies fell in a range from 0.0101 in to 0.0104 in.

The average stress and strain for the initial crack in this lay-up were found to be 4.440 ksi and 2ο9 με, respectively. In all of the specimens that were analyzed for crack initiation transverse cracks appeared in both 90° plies at the same stress levels, but the initial crack densities were different (see Table 6). Once again, the initial transverse cracks developed near the 0°/90° ply interface, progressed through the 90° plies in a direction perpendicular to the load, and were constrained by the 0° plies.

C. Discussion of Results

Many similarities were seen in the behavior of the four lay-ups studied. With the exception of the $0/90/0_4/90/0$ lay-up, all of the stress-strain curves were relatively linear to failure. The stress-strain curves for the $0/90/0_4/90/0$ specimens had a slight reduction in modulus at applied

Table 6
Stress, Strain and Crack Spacing for $0/90/0_4/90/0$ Lay-up

Specimen	Stress (ksi)	Strain (%)	Crack Spacing in First 90° Ply (in)	Crack Spacing in Second 90° Ply (in)
90C30-01	3.862	0.0242	0.1875	0.7500
	7.241	0.0479	0.0491	0.1719
	9.655	0.0640	0.0269	0.0558
	12.117	0.0791	0.0174	0.0319
	15.689	0.1053	0.0150	0.0240
	19.310	0.1324	0.0160	0.0187
	27.807	0.2054	0.0130	0.0149
	31.427	0.2462	0.0125	0.0131
	35.144	0.2947	0.0111	0.0115
	39.393	0.3458	0.0108	0.0104
	48.275	0.4371	0.0104	0.0104
90C30-02	4.878	0.0305	0.2656	0.5313
	7.174	0.0462	0.0480	0.0611
	10.760	0.0711	0.0215	0.0344
	14.395	0.0960	0.0206	0.0275
	19.177	0.1311	0.0163	0.0166
	23.960	0.1653	0.0138	0.0141
	28.742	0.2005	0.0126	0.0124
	33.477	0.2552	0.0111	0.0111
	38.259	0.3465	0.0101	0.0101
	43.042	0.4327	0.0103	0.0101
	47.824	0.4991	0.0101	0.0101

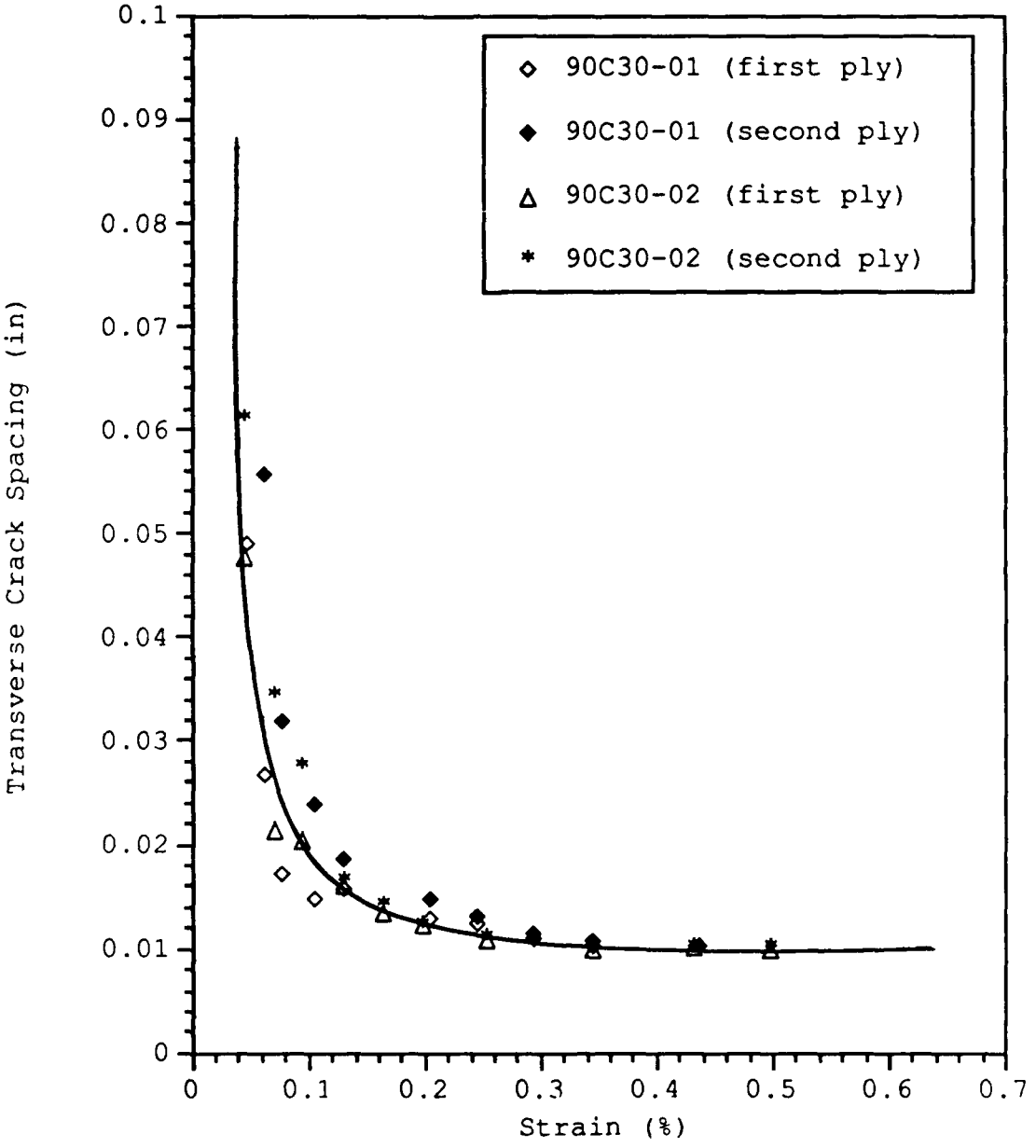

Figure 25. Crack Spacing as a Function of Strain for $0/90/0_4/90/0$

stresses between 25 and 30 ksi. The transverse cracks always formed at the $0^{\circ}/90^{\circ}$ ply interface and progressed straight through the 90° ply in a direction relatively perpendicular to the applied load. At higher stress levels crack branching was common and longitudinal cracks formed, joining the transverse cracks. The longitudinal cracks were quite prevalent in the three lay-ups with the 90° plies in the center, less so in the $0/90/0_4/90/0$ lay-up. Wang and Parvizi-Majidi also reported the occurrence of these longitudinal cracks in fiber reinforced ceramic matrix composites (3). It is believed that the longitudinal cracks are caused by the Poisson's effect. As a result of the transverse cracking, a region of the 90° ply on either side of each crack unloads. This unloading tends to release the Poisson's contraction of the ply in the thickness direction near the crack. However, this deformation is inhibited by the portion of the 90° ply between the transverse cracks which is still carrying load. As a result, stresses develop in the 90° ply along the thickness direction. These stresses are compressive near the cracks and tensile in the region between the cracks. The tensile component of the stress leads to the development of the longitudinal cracks.

In all of the lay-ups except the $0_3/90_3/0_3$, the transverse cracking was constrained by the 0° plies and the cracks travelled only a few fiber diameters into the 0° plies. At low stress, the 0° plies did constrain the

transverse cracks in the $0_3/90_3/0_3$ lay-up. However, as the stress level was increased, some of the transverse cracks penetrated the 0° plies and began to travel in the longitudinal direction. This was shown in Figure 20. It is believed that this phenomenon is related to the thickness of the transverse ply, but further investigation is needed.

As mentioned in Chapter II, the following transverse cracking behavior has been noted by other researchers in relation to polymer based composites: (a) for a given strain, the crack spacing increased as the transverse ply thickness was increased; (b) the saturation crack spacing decreased as the transverse ply thickness decreased; and (c) the strain for the onset of transverse cracking increased as the transverse ply thickness decreased. These same phenomena were seen in the tested fiber reinforced ceramic matrix composite. Figure 26 is a graph of the crack spacing as a function of percent strain for the three lay-ups with the transverse plies in the center of the laminate. The occurrence of (a) and (b) can clearly be seen. For a given strain, the crack spacing did increase as the transverse ply thickness increased and the saturation crack spacing can be seen to decrease as the transverse ply thickness decreases. Table 7 and Figure 27 verify the occurrence of (c); the average value of the strain that caused crack initiation did increase as the transverse ply thickness decreased. Table 7 also shows the saturation crack spacings and crack initiation

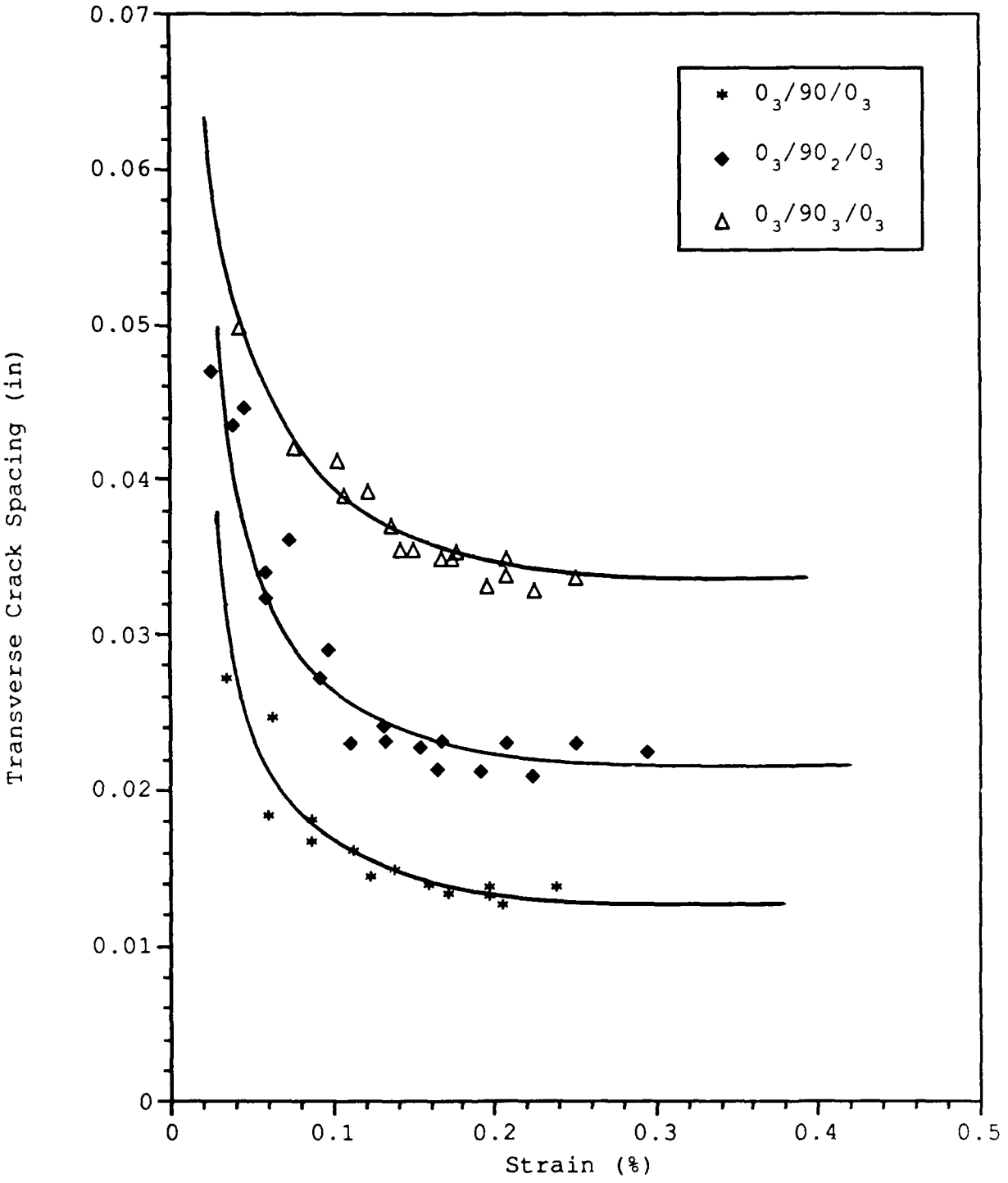

Figure 26. Crack Spacing as a Function of Strain and Transverse Ply Thickness

strains that were seen by Wang and Parvizi-Majidi (3) in a similar fiber reinforced ceramic matrix composite (SiC/CAS). The crack spacings observed by Wang and Parvizi-Majidi are nearly identical to those found for the SiC/1723, while the initiation strains show some difference in value but similar trends. In Figure 27 it can be seen that as the number of 90° plies was increased, the strain for crack initiation in the cross-ply laminates approached the value for a 90° lamina. This happens as the thickness of the transverse ply overcomes the constraining effects of the longitudinal plies.

As previously mentioned, the fourth lay-up ($0/90/0_4/90/0$) was used to study the effect of the placement of the 90° plies. It was expected that this lay-up would yield results similar to the $0_3/90/0_3$ lay-up because of the

Table 7
Average Saturation Crack Spacing and Crack Initiation Stress for Varying Number of Transverse Plies

Number of Transverse Plies	Average Saturation Crack Spacing (in)		Average Strain for Crack Initiation (με)		Avg Stress for Crack Initiation (ksi)
	SiC/1723	SiC/CAS	SiC/1723	SiC/CAS	
1	0.013	0.013	331	500	5.01
2	0.022	0.026	277	250	4.80
3	0.034	0.035	273	120	4.07

Data for SiC/CAS from Wang and Parvizi-Majidi (3)

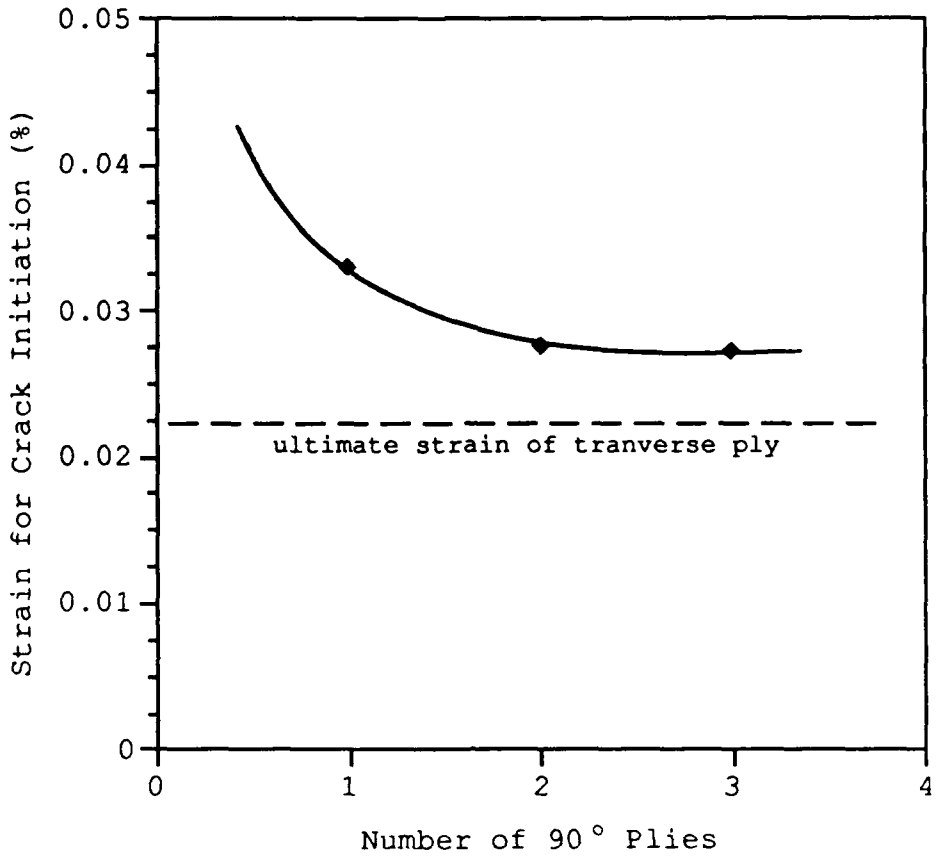

Figure 27. Variation of the Crack Initiation Strain with the Thickness of the Transverse Ply

constraining 0° plies on both sides of the 90° plies. The average saturation crack spacing of these two lay-ups did compare quite well (0.010 in for the $0/90/0_4/90/0$ and 0.013 in for the $0_3/90/0_3$). However, there was some difference in the stress and strain for crack initiation (4.44 ksi/289 με for the $0/90/0_4/90/0$ and 5.01 ksi/331 με for the $0_3/90/0_3$). This result was not unexpected. Cracks initiated in the $0/90/0_4/90/0$ laminate at lower stress and strain levels

because the transverse ply in that lay-up has less constraint than does the $0_3/90/0_3$. Further studies with other distributed 90° ply lay-ups are needed to fully characterize the effect of the location of the 90° plies. Figure 28 provides a comparison of the crack spacing in the $0/90/0_4/90/0$ lay-up to that in the $0_3/90/0_3$ lay-up.

As previously stated, most of the specimens broke in the gage length. Delamination was not evident except in three of the five specimens of the $0_3/90_3/0_3$ lay-up. Figure 29 provides a representative sample of a fractured specimen from each lay-up.

D. Comparison to Theoretical Models

This section will compare the test results with the theoretical models outlined in Chapter II. The predicted values for the crack initiation stress and the first ply failure stress will be compared to the stress values that caused the first cracking in the four lay-ups. The predicted values for the modulus of elasticity will be compared to the experimentally observed values. Finally, the predicted crack density will be compared to the actual crack density. It should be noted that the theoretical crack density model outlined in Chapter II is only valid for a cross-ply laminate with a transverse ply between two equally thick longitudinal plies. Thus, the theory had to be modified to allow the

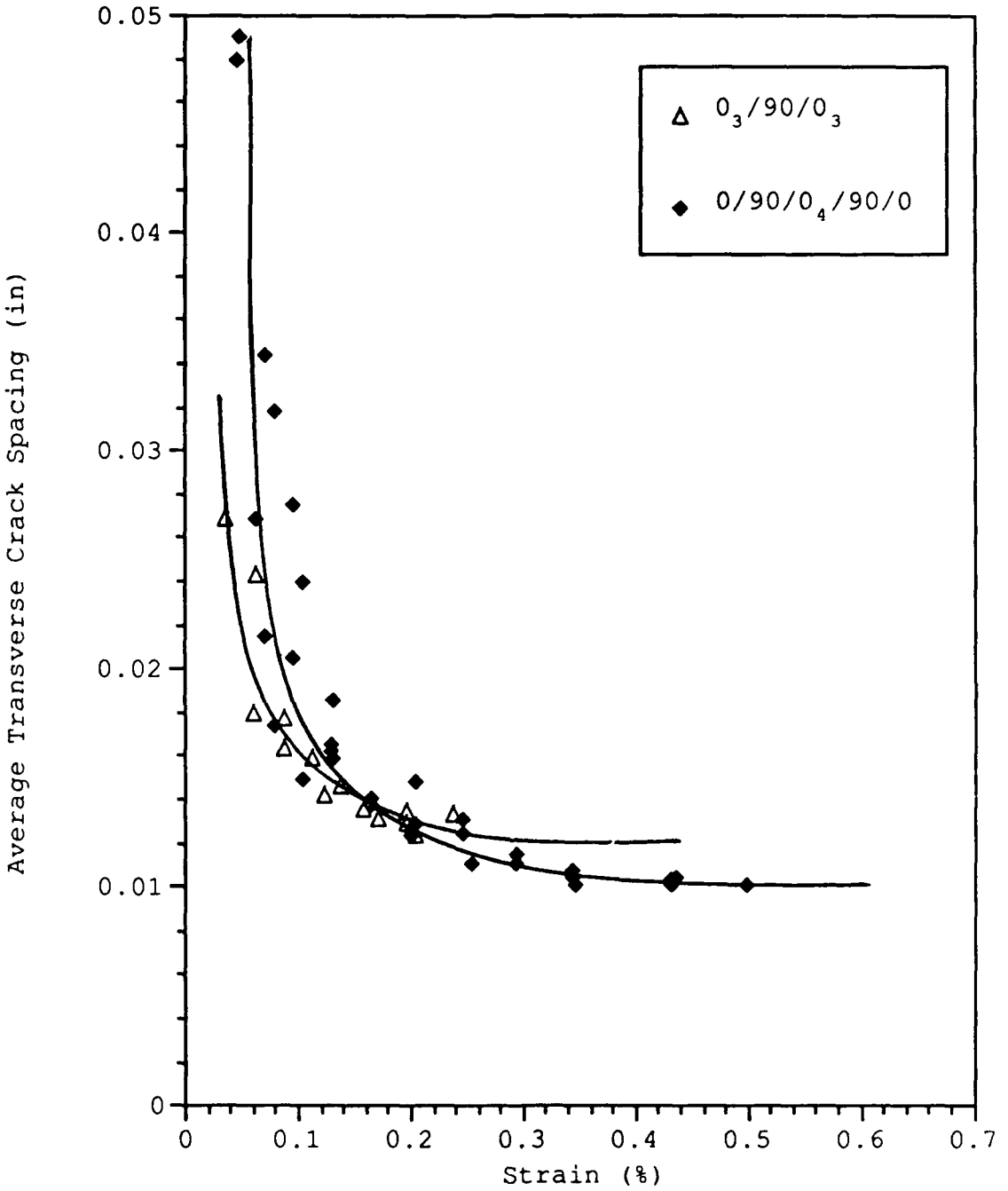

Figure 28. Comparison of Crack Spacing in $0_3/90/0_3$ to $0/90/0_4/90/0$

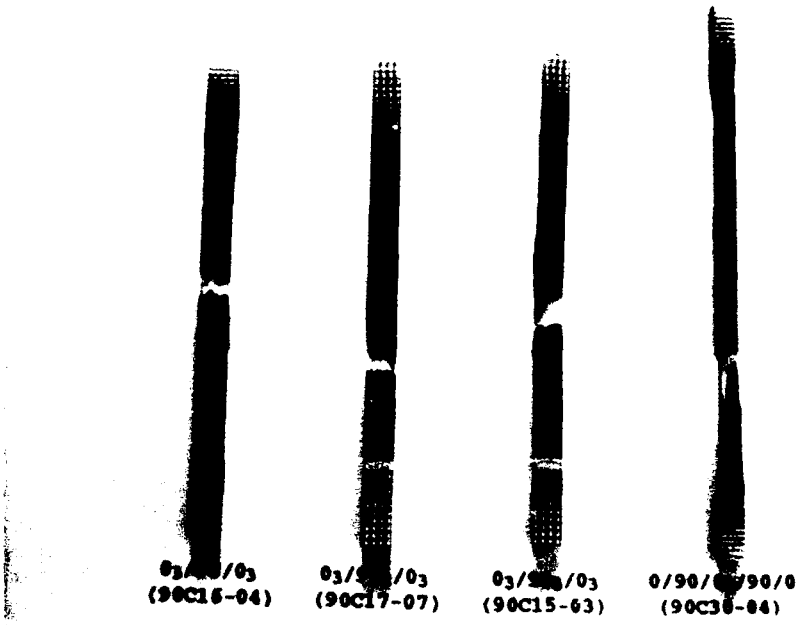

Figure 29. Broken Specimens From Each Lay-up

calculation of the theoretical crack density of the $0/90/0_4/90/0$ lay-up. Because of symmetry it was decided to model one half of the $0/90/0_4/90/0$ lay-up as a $0/90/0_2$ laminate. Garrett and Bailey's theory was then applied twice, once for a 0/90/0 and once for a $0_2/90/0_2$. The results of these two calculations were then averaged, providing a theoretical crack spacing for the $0/90/0_4/90/0$ lay-up.

1. Crack Initiation and First Ply Failure Prediction

In Chapter II, two theories for predicting crack initiation stresses were presented. The first theory

proposed that the transverse ply has a unique breaking strain and that the first crack would occur at the stress level yielded by Eq (1). As noted in Chapter III, the breaking strain of the transverse ply was assumed to be 217 με. Using Eqs (2) through (19), the first ply failure theory was also used to predict the stress level for crack initiation. The complete first ply failure analysis is shown in the appendix. Table 8 provides a comparison of the stress levels predicted by Eq (1), the first ply failure theory, and those actually observed in the testing. Two values are presented for the predicted initiation stress, one based on the experimental modulus of elasticity values and the other based on the theoretical modulus values. As can be seen in the table, the experimentally observed stress levels are all somewhat higher

Table 8
Comparison of Experimental and Predicted Crack Initiation Stresses

Lay-up	Experimental Initiation Stress (ksi)	Predicted Initiation Stress (ksi)		Predicted First Ply Failure Stress (ksi)
		Exp Mod	Theo Mod	
$0_3/90/0_3$	5.01	3.90	4.17	4.22
$0_3/90_2/0_3$	4.80	3.43	4.00	4.03
$0_3/90_3/0_3$	4.07	2.97	3.86	3.89
$0/90/0_4/90/0$	4.44	3.32	4.00	3.93

than the predicted values. Mall and Kim (14:734) ran similar tests on SiC/CAS III and also reported crack initiation stresses considerably higher than predicted. Several possible explanations for this disagreement are given. Firstly, assumed values for the shear modulus (G_{12}) and the transverse strength were used in calculating the predicted values. Secondly, it was assumed that the laminate was in an initial stress free state, i.e. no curing stresses were present in the laminate. This could possibly be too simplistic an approach in ceramic composites and is the most likely cause of the difference between the predicted and actual crack initiation stresses.

2. Modulus of Elasticity Prediction

In Chapter II it was shown that it is possible to predict the modulus of elasticity of a laminate by using the results of the first ply failure analysis and Eq (20). These calculations are shown in detail in the appendix. Table 9 presents a comparison of the experimentally obtained values of the modulus of elasticity to the theoretical values before and after first ply failure. In all cases, the predicted modulus is larger than the experimentally observed value. The most likely cause of this discrepancy is the use of the assumed unidirectional lamina values for E_1, E_2, and G_{12}. Assumed values were used because no unidirectional specimens were available for testing.

Table 9
Comparison of Experimental and Theoretical Modulus of Elasticity

Lay-up	Experimental Modulus (msi)	Predicted Modulus (msi)	Predicted Modulus After FPF (msi)
$0_3/90/0_3$	17.96	19.23	17.40
$0_3/90_2/0_3$	15.82	18.43	15.23
$0_3/90_3/0_3$	13.70	17.80	13.53
$0/90/0_4/90/0$	15.30	18.43	15.23

Having values for the modulus of elasticity before and after first ply failure allows theoretical stress-strain curves to be developed. The theoretical stress-strain curves are bi-linear, with an initial slope equal to the modulus of elasticity prior to first ply failure and a final slope equal to the modulus of elasticity after first ply failure. Figures 30-33 present comparisons of the experimental stress-strain curves to the theoretical curves for each of the tested lay-ups. Also shown in the figures is a comparison of the experimental and the theoretical point for first ply failure. Good agreement between the theoretical and experimental curves was noted. However, at higher stress values the $0/90/0_4/90/0$ lay-up showed considerable non-linearity that was not predicted. As was previously discussed with relation to the experimental curves, the theoretical stress-strain curves did not have dramatic changes in slope after first ply failure.

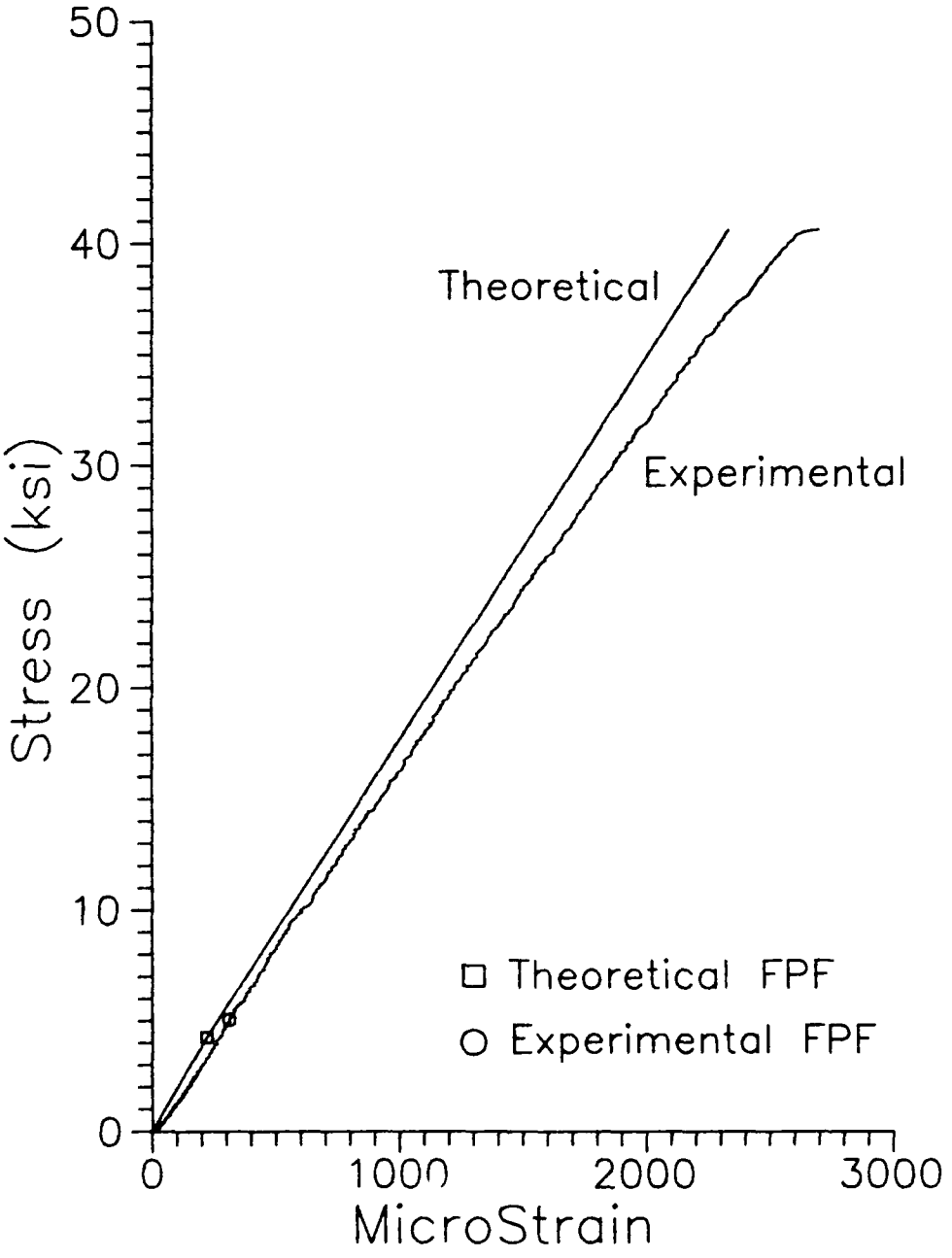

Figure 30. Experimental and Theoretical Stress-Strain Curves For $0_3/90/0_3$ (Specimen 90C16-01)

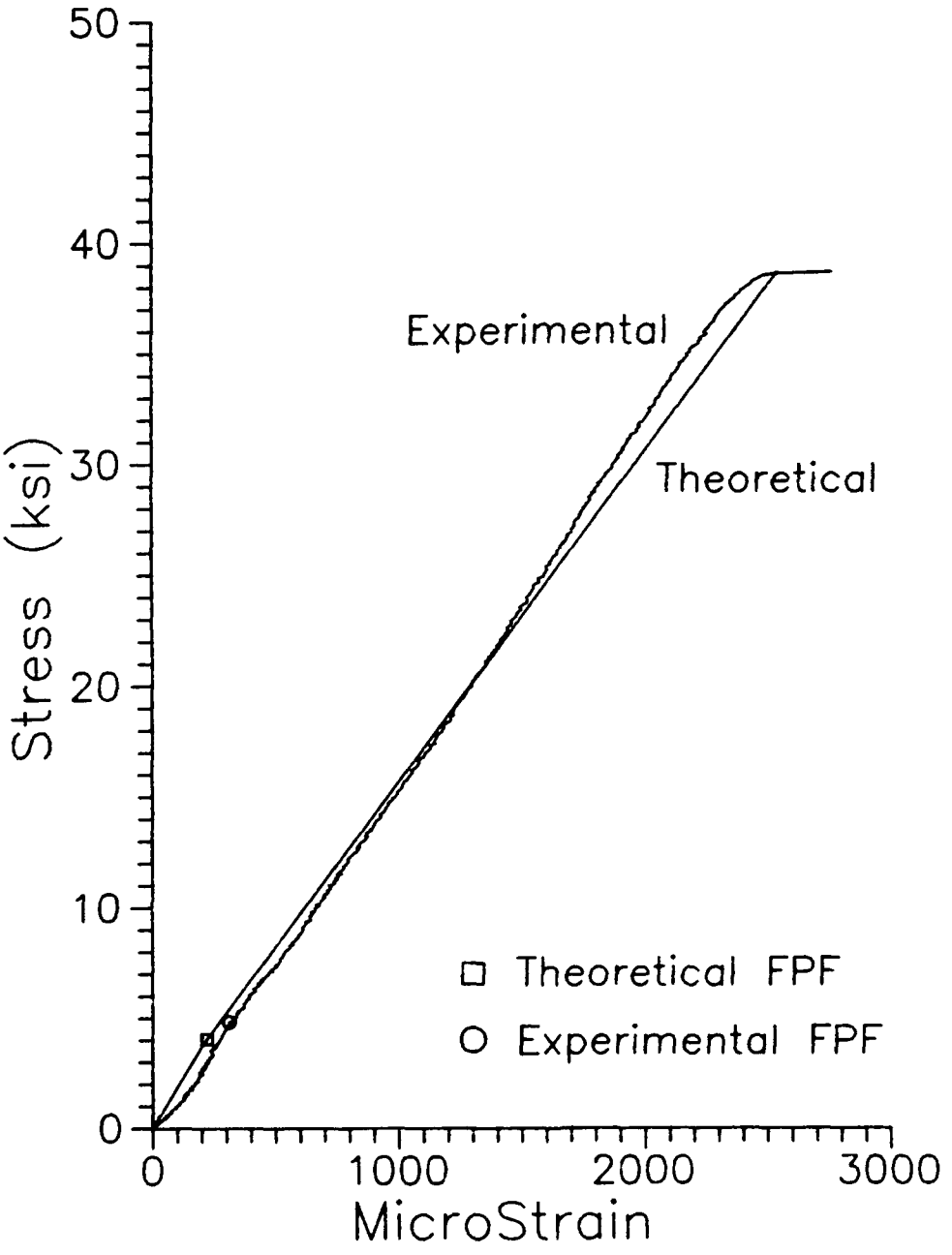

Figure 31. Experimental and Theoretical Stress-Strain Curves For $0_3/90_2/0_3$ (Specimen 90C17-09)

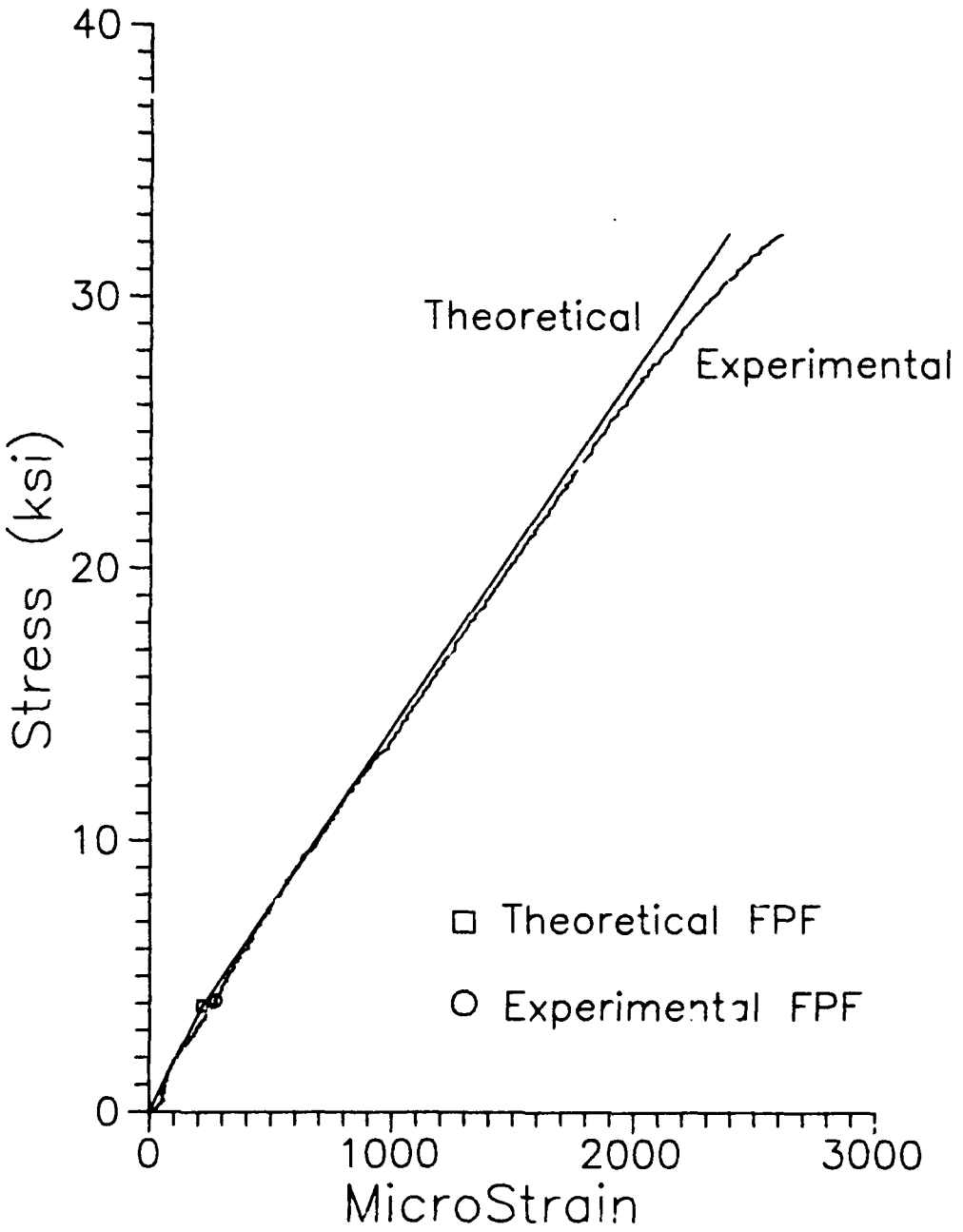

Figure 32. Experimental and Theoretical Stress-Strain Curves For $0_3/90_3/0_3$ (Specimen 90C15-02)

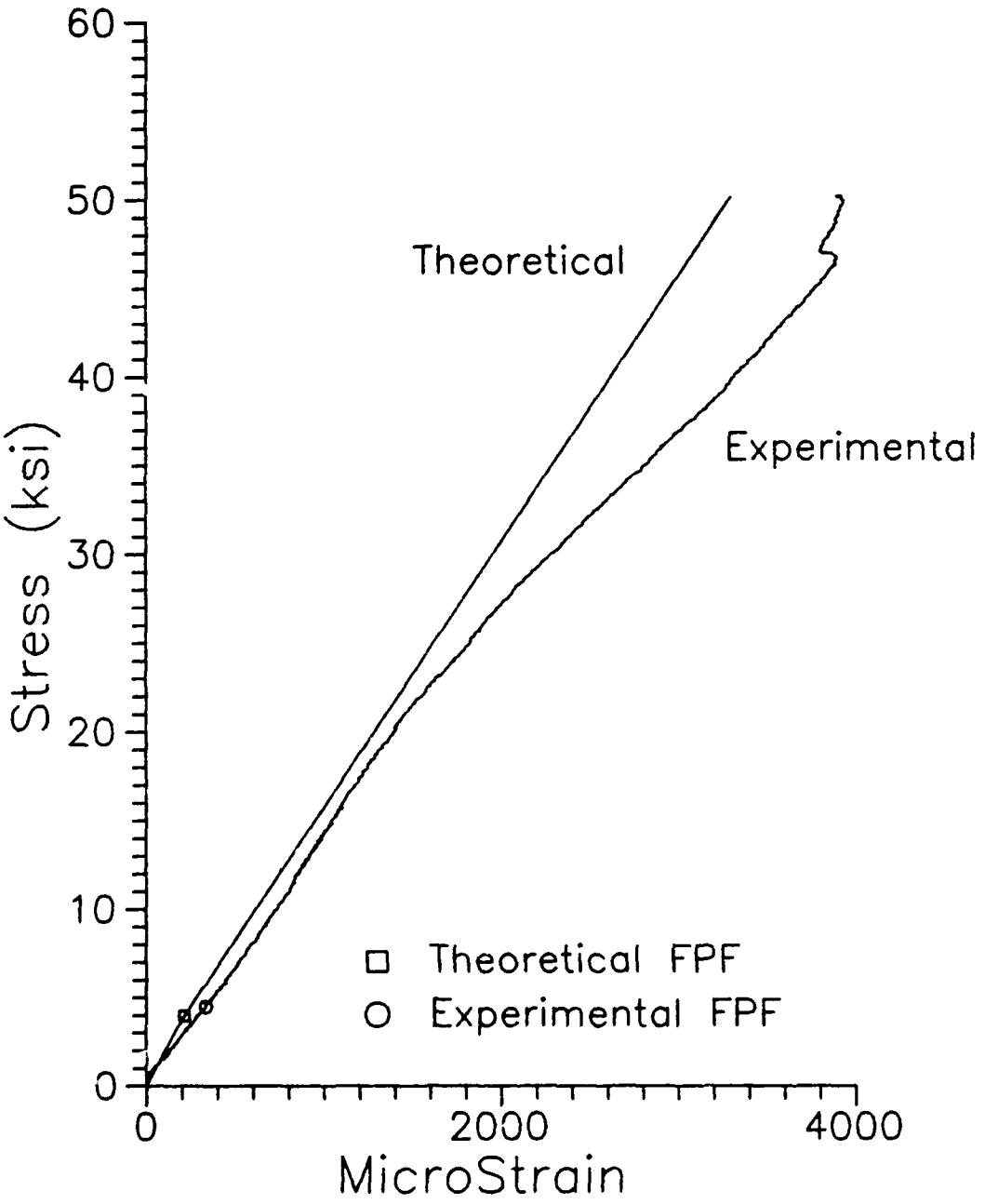

Figure 33. Experimental and Theoretical Stress-Strain Curves For $0/90/0_4/90/0$ (Specimen 90C30-03)

3. Saturation Crack Spacing Prediction

The theoretical model proposed by Garrett and Bailey (1:162) and outlined in Chapter II was used to predict the saturation crack spacing in the four tested cross-ply laminates. As was stated in Chapter II, the application of this theory results in a stepped curve for crack spacing versus applied stress. Figures 34 to 37 show the comparison between the experimental results for the four lay-ups and the theoretical prediction of crack spacing. The modeling of the fourth lay-up ($0/90/0_4/90/0$) had to be modified because its geometry did not match the requirement for Garrett and Bailey's theory (i.e., it did not have a single transverse ply between two equally thick longitudinal plies). Thus, the $0/90/0_4/90/0$ was modeled as a $0/90/0_2$ (cutting the laminate along the line of symmetry). Because this approach still did not satisfy the required geometrical limitations, it was assumed that the theoretical crack spacing for a $0/90/0_2$ laminate would fall between the theoretical spacing for a $0/90/0$ and a $0_2/90/0_2$. Therefore, the theoretical spacing shown for the $0/90/0_4/90/0$ lay-up in Figure 37 is the average of the theoretical spacings for a $0/90/0$ lay-up and a $0_2/90/0_2$ lay-up. As can be seen from Figures 34 to 37, the observed crack spacing is always higher than that predicted by the theory. The large discrepancy between the predicted and the experimental crack spacing when using shear lag analysis has also been noted by other researchers. Garrett and Bailey

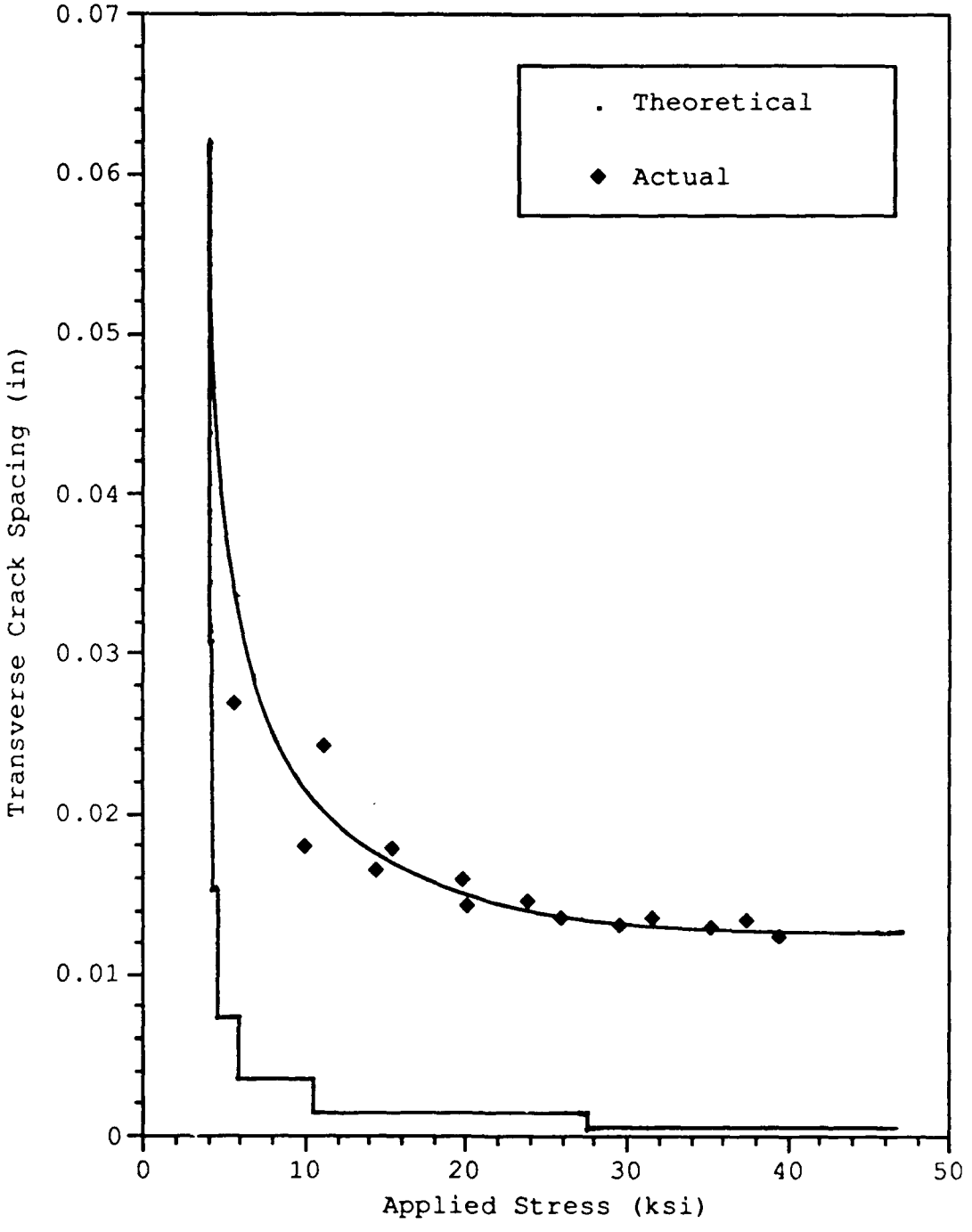

Figure 34. Observed versus Theoretical Crack Spacing in $0_3/90/0_3$

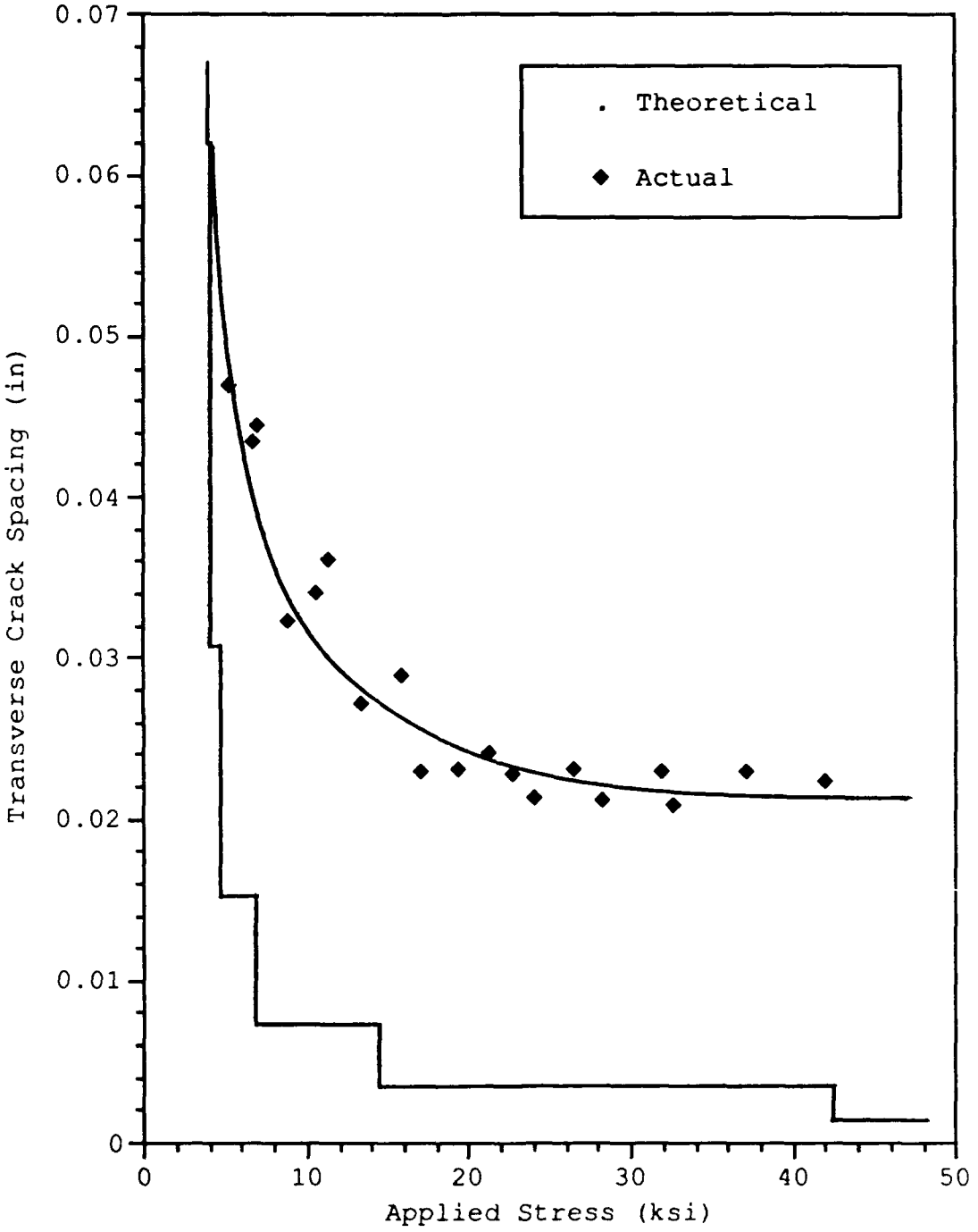

Figure 35. Observed versus Theoretical Crack Spacing in $0_3/90_2/0_3$

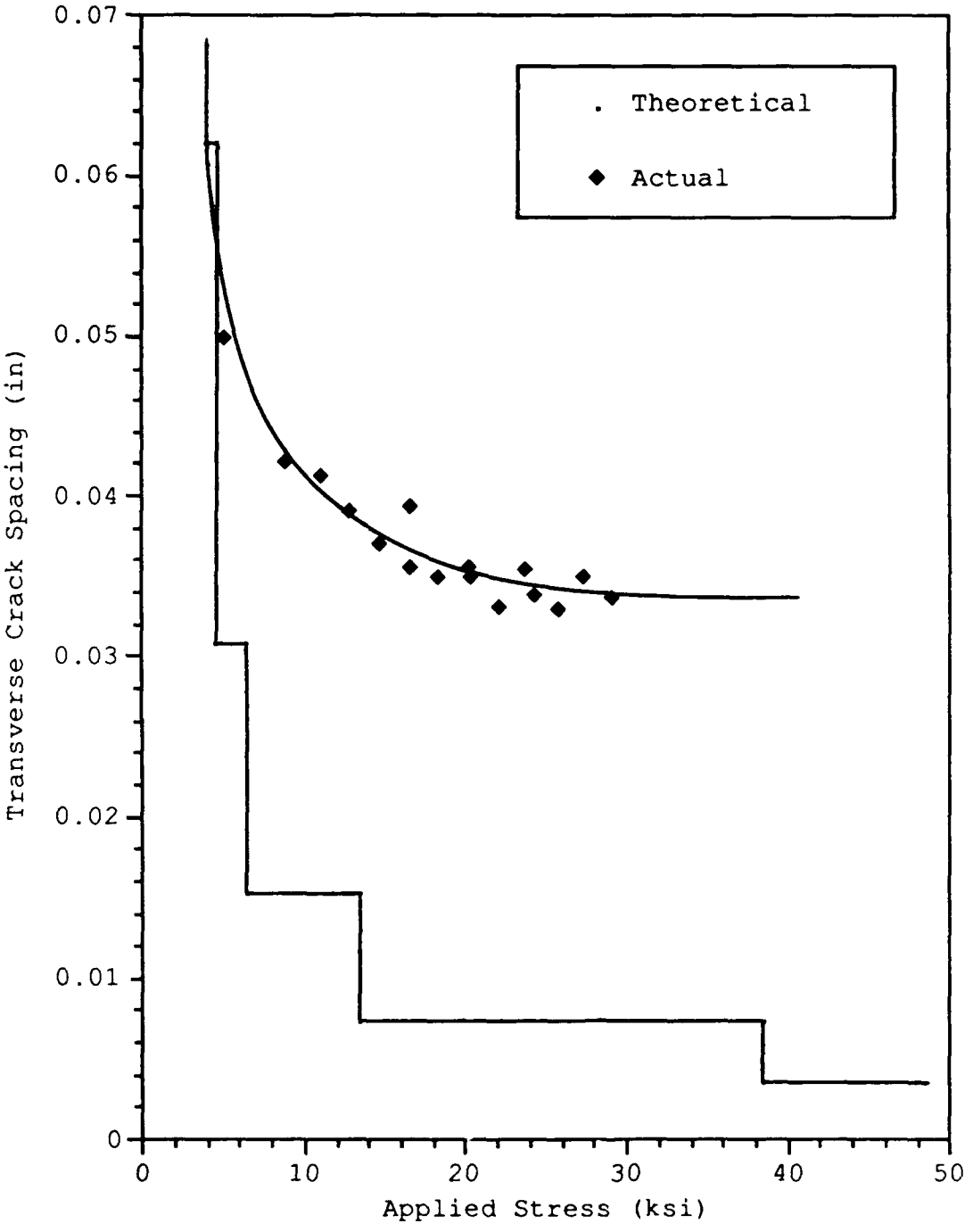

Figure 36. Observed versus Theoretical Crack Spacing in $0_3/90_3/0_3$

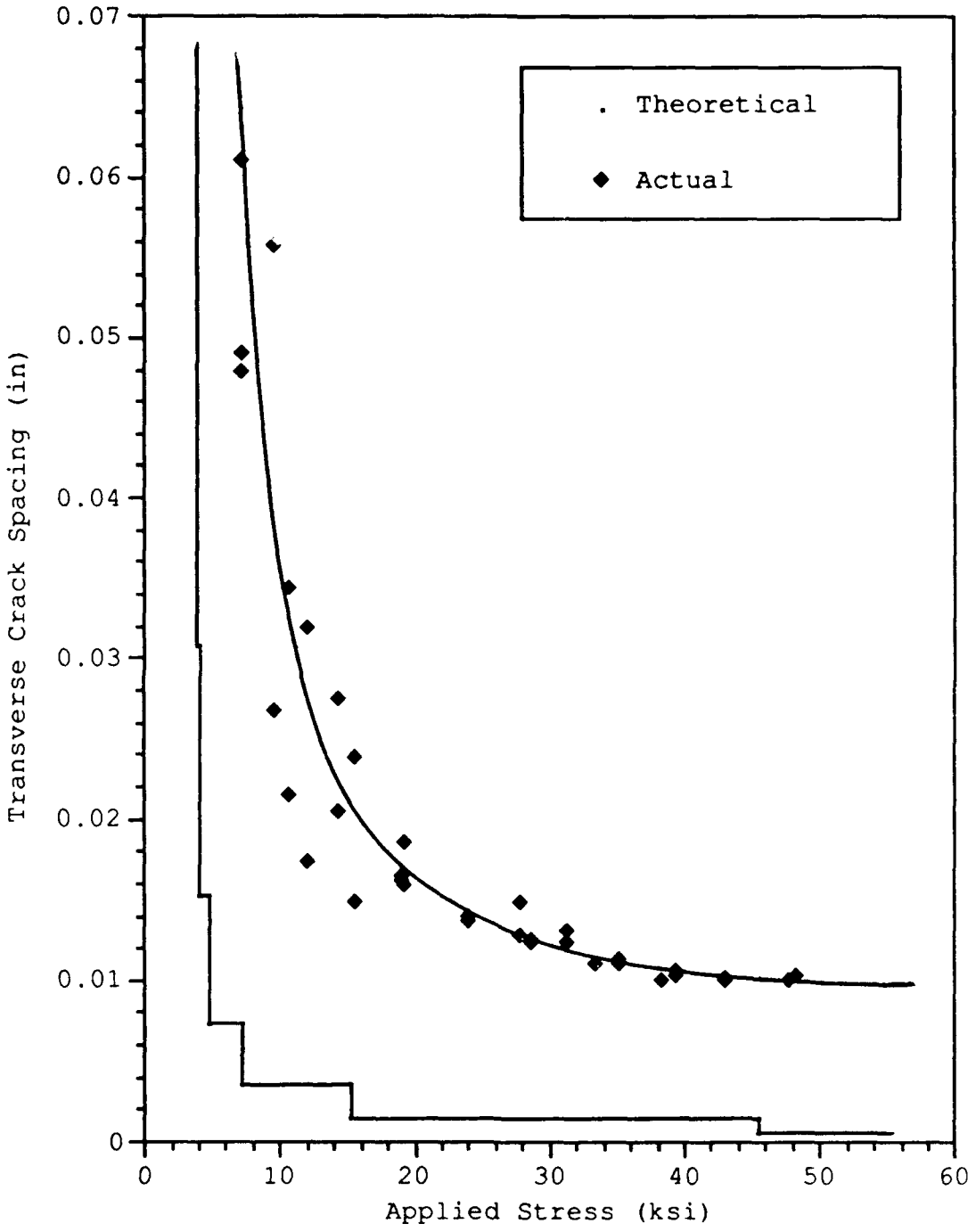

Figure 37. Observed versus Theoretical Crack Spacing in $0/90/0_4/90/0$

(1:166) observed this discrepancy in a glass/epoxy system. Kim (15:19-3) and Sun and Jen (5:213-214) noted the same phenomenon in graphite/epoxy. Nevertheless, the theory does supply the general form of the experimental results, with the observed effect of the increase in crack spacing with increasing ply thickness clearly visible in the figures. It is interesting to note that the theoretical crack spacing for the $0/90/0_4/90/0$ lay-up falls just below the theoretical spacing for the $0_3/90/0_3$ lay-up. This is the same phenomenon that was seen in the experimental data.

E. Comparison with Other Composite Systems

In this section, the experimental results obtained for the SiC/1723 will be compared to similar works with glass/epoxy and graphite/epoxy systems. Comparisons of saturation crack spacing and crack initiation strain will be made.

Kim (15:19-3) ran tests on $[0/90_n]_s$ laminates of graphite/epoxy where the number of 90° plies was varied from one to six. He observed that as the number of 90° plies was increased, the number of cracks per inch at the limiting case (saturation) deceased. This is the same result that was observed for the SiC/1723 ceramic composite. Tests on a glass/epoxy system were run by Garrett and Bailey (1:160) using $0/90_n/0$ lay-ups. They also observed that the number of cracks per inch at saturation deceased as the thickness of the transverse ply was increased. Figure 38 is a comparison

of the saturation crack density for the three composite systems (SiC/1723, graphite/epoxy and glass/epoxy) as a function of the number of 90° plies. It should be noted that the curves for the SiC/1723 and the graphite/epoxy have nearly identical slopes, while the glass/epoxy curve is considerably flatter.

A comparison of the three composite systems can also be made in relation to the strain for crack initiation. Once again, data from Kim (15:19-3) and Garrett and Bailey (1:161) were used for the graphite/epoxy and glass/epoxy, respectively. Figure 39 presents the percent strain for crack initiation versus the number of 90° plies for the three composite systems. As should be expected, the brittle matrix of the SiC/1723 results in a much lower strain for crack initiation.

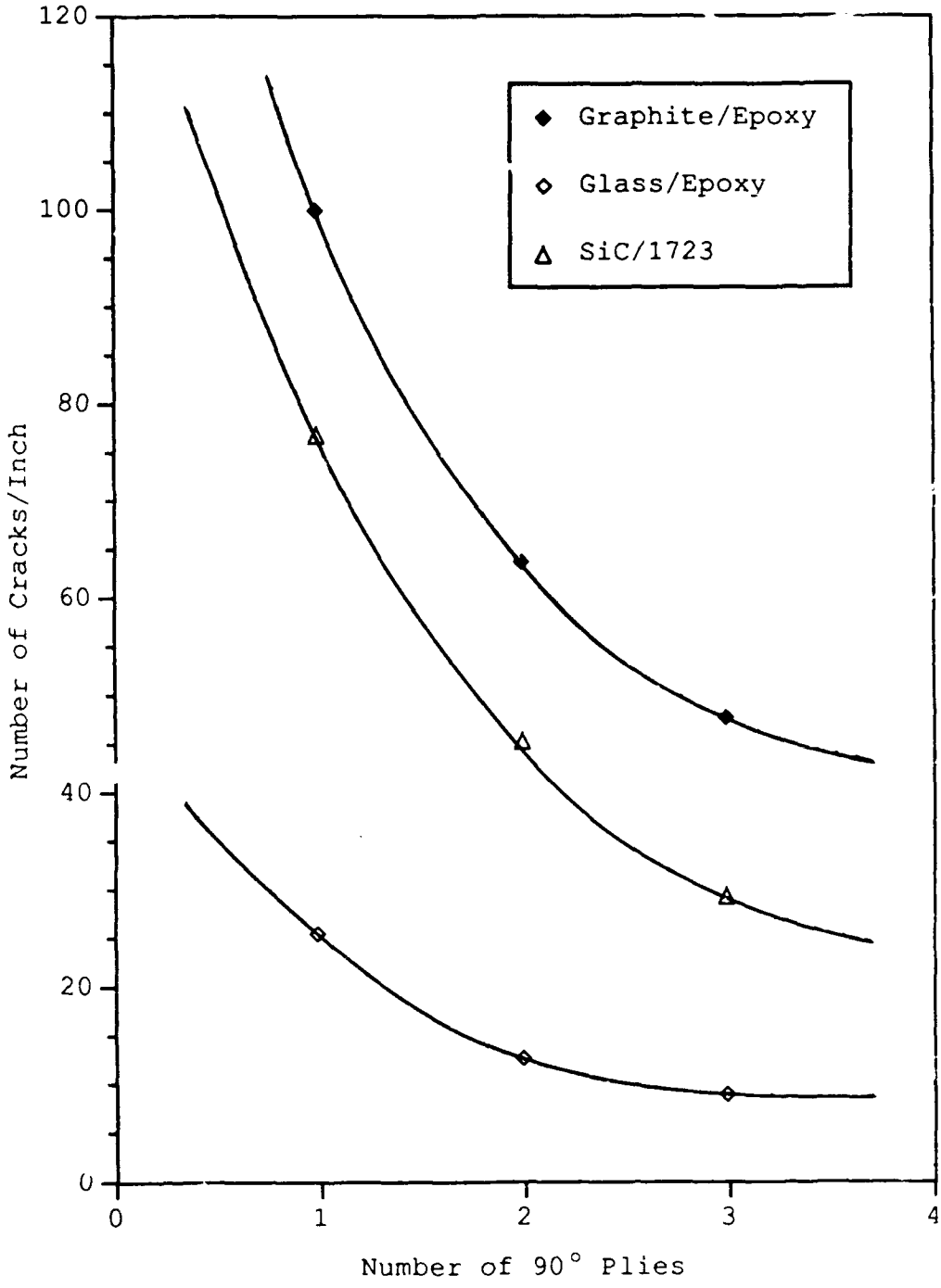

Figure 38 Effects of the 90° Ply Thickness and the Composite System on the Crack Density at the Limiting Case

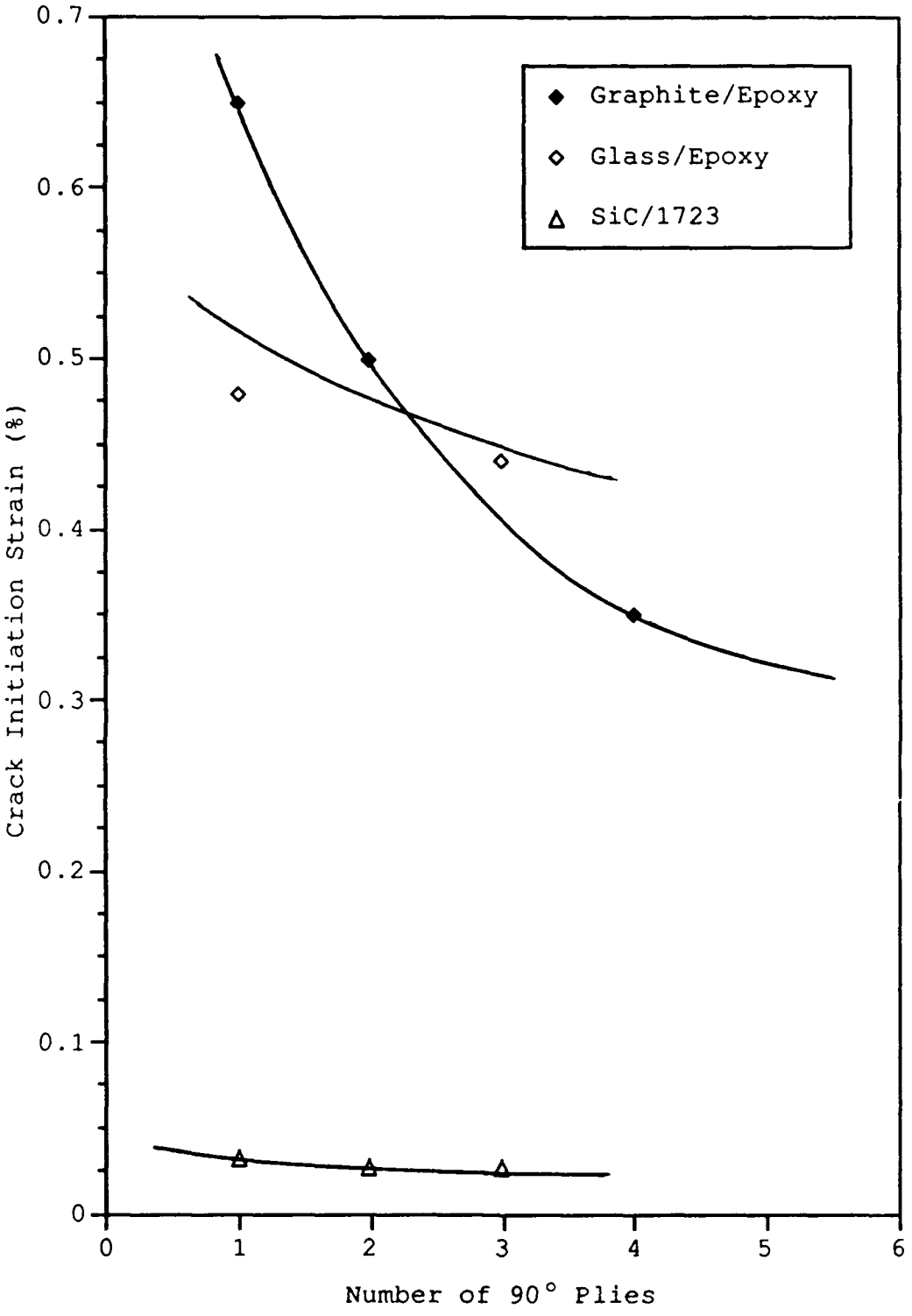

Figure 39. Variation of the Crack Initiation Strain with the Thickness of the Transverse Plies and the Composite System

V. Conclusions

The primary goal of this study was to gain an understanding of the correlation between crack initiation stress and strain, saturation crack spacing and transverse ply geometry in cross-ply laminates of a fiber reinforced ceramic matrix composite. Three different $0_3/90_n/0_3$ lay-ups were tested to determine the effect of the transverse ply thickness and a $0/90/0_4/90/0$ lay-up was tested to observe the effects of the transverse ply location. The specimens were tested in uniaxial tension and transverse cracking behavior was analyzed. Acoustic emission was used in conjunction with replication to determine the stress levels for crack initiation. Replication was used to monitor crack progression and calculate crack densities. Strain gages were used to collect axial and transverse strain as function of applied stress. Theoretical models for crack initiation, Young's modulus and crack density were presented and the experimental data were compared to the theoretical predictions. Finally, the cracking behavior of the ceramic matrix composite was compared to graphite/epoxy and glass/epoxy systems. The conclusions drawn from this study are as follows:

1. In this material, acoustic emission is a useful tool for determining the stress level for transverse crack initiation. However, it is essential that replication be used to confirm that cracking has begun. The replications must be made while the specimen is loaded so that the cracks will remain open.

2. Transverse cracking developed in the 90° plies at relatively low stress levels. The cracks generally formed at the $0^{\circ}/90^{\circ}$ ply interface and progressed straight through the 90° ply, perpendicular to the applied load. As the applied load was increased more cracks formed, evenly spaced along the length of the 90° ply.

3. The transverse cracks were totally constrained by the 0° plies in all of lay-ups except for the $0_3/90_3/0_3$. At stress levels above 10 ksi, some of the transverse cracks in the $0_3/90_3/0_3$ lay-up penetrated the 0° plies and began to travel in the longitudinal direction at the $0^{\circ}/90^{\circ}$ ply interface. It is believed that these cracks were responsible for partial delamination in three of the five specimens of this lay-up.

4. After the transverse cracks had developed, longitudinal cracks formed in the 90° plies, joining the transverse cracks. This behavior was noted in all of the lay-ups, but was less prevalent in the $0/90/0_4/90/0$ laminate.

5. For a given strain, the crack spacing increased as the transverse ply thickness was increased.

6. The saturation crack spacing decreased (i.e., the cracks were closer together) as the transverse ply thickness was decreased.

7. The strain for the onset of transverse cracking increased as the transverse ply thickness was decreased.

8. The saturation crack spacing of the $0/90/0_4/90/0$ lay-up was similar to the $0_3/90/0_3$ lay-up, while the crack initiation stress and strain were somewhat lower. This is due to the fact that the 90° plies in the $0/90/0_4/90/0$ lay-up have less constraint than in the $0_3/90/0_3$.

9. The use of classical laminate theory resulted in predicted crack initiation stresses that were lower than the experimentally observed values. The assumption of an initially stress free state (i.e., no curing stresses) is the most likely cause of the differences.

10. The modulus of elasticity values predicted by classical laminate theory were somewhat higher than the experimentally determined values. The most likely cause of the differences is the use of assumed values for unidirectional properties of SiC/1723.

11. A theory proposed by Garrett and Bailey (1:162) was used to predict saturation crack spacing. The observed crack spacing was always higher than that predicted by the theory. However, the theory was useful in predicting general crack spacing trends.

12. Saturation crack spacing in SiC/1723 was shown to follow the same trends as in glass/epoxy and graphite/epoxy. However, because of its brittle matrix, transverse cracking in SiC/1723 begins at a much lower strain than in glass/epoxy or graphite/epoxy.

VI. Recommendations

While much has been learned about transverse cracking in a fiber reinforced ceramic composite, there are a number of areas that warrant further investigation. Among the areas that deserve further consideration are the following.

1. The effect of transverse ply thickness on delamination at the $0^{\circ}/90^{\circ}$ ply interface should be investigated by testing lay-ups with transverse plies thicker than the $0_3/90_3/0_3$.
2. Additional testing of other lay-ups with distributed 90° plies should be done in an attempt to characterize the effect of the transverse ply location on crack initiation stress and crack spacing.
3. Other theories for crack spacing should be investigated, including those of Laws and Dvorak (9:906-909) and Wang and Crossman (10:76-83).
4. Finally, it would be interesting to study the effects of thermal and/or load cycling on the transverse cracking behavior of ceramic composites. Tests at elevated temperatures would be especially important, as these ceramic composites are anticipated to be used in high temperature applications.

Appendix: Sample Calculations

Sample calculations for the predictions of the first ply failure stress and the modulus of elasticity will be presented in this section. The sample calculations are provided for the $0_3/90/0_3$ lay-up, but the procedures are the same for all of the lay-ups.

A. Predicted First Ply Failure Stress Calculations

The following SiC/1723 lamina property values were used:

$$E_1 = 20{,}300 \text{ ksi}$$
$$E_2 = 12{,}760 \text{ ksi}$$
$$G_{12} = 20{,}300 \text{ ksi}$$
$$\nu_{12} = 0.18$$

From Eq (2), $\nu_{21} = 0.113$.

From Eq (4), the reduced stiffness matrix is

$$[Q] = \begin{bmatrix} 20722 & 2344.6 & 0 \\ 2344.6 & 13025.3 & 0 \\ 0 & 0 & 6381 \end{bmatrix} \text{ ksi}$$

From Eq (6), the transformed reduced stiffness matrices for the 0° and 90° plies are

$$[Q]_0 = \begin{bmatrix} 20722 & 2344.6 & 0 \\ 2344.6 & 13025.3 & 0 \\ 0 & 0 & 6381 \end{bmatrix} \text{ ksi}$$

and

$$[Q]_{90} = \begin{bmatrix} 13025.3 & 2344.6 & 0 \\ 2344.6 & 20722 & 0 \\ 0 & 0 & 6381 \end{bmatrix} \text{ ksi}$$

Figure 35 provides the laminate geometry, where

$h_0 = -0.035$ in $\quad h_4 = 0.005$ in
$h_1 = -0.025$ in $\quad h_5 = 0.015$ in
$h_2 = -0.015$ in $\quad h_6 = 0.025$ in
$h_3 = -0.005$ in $\quad h_7 = 0.035$ in

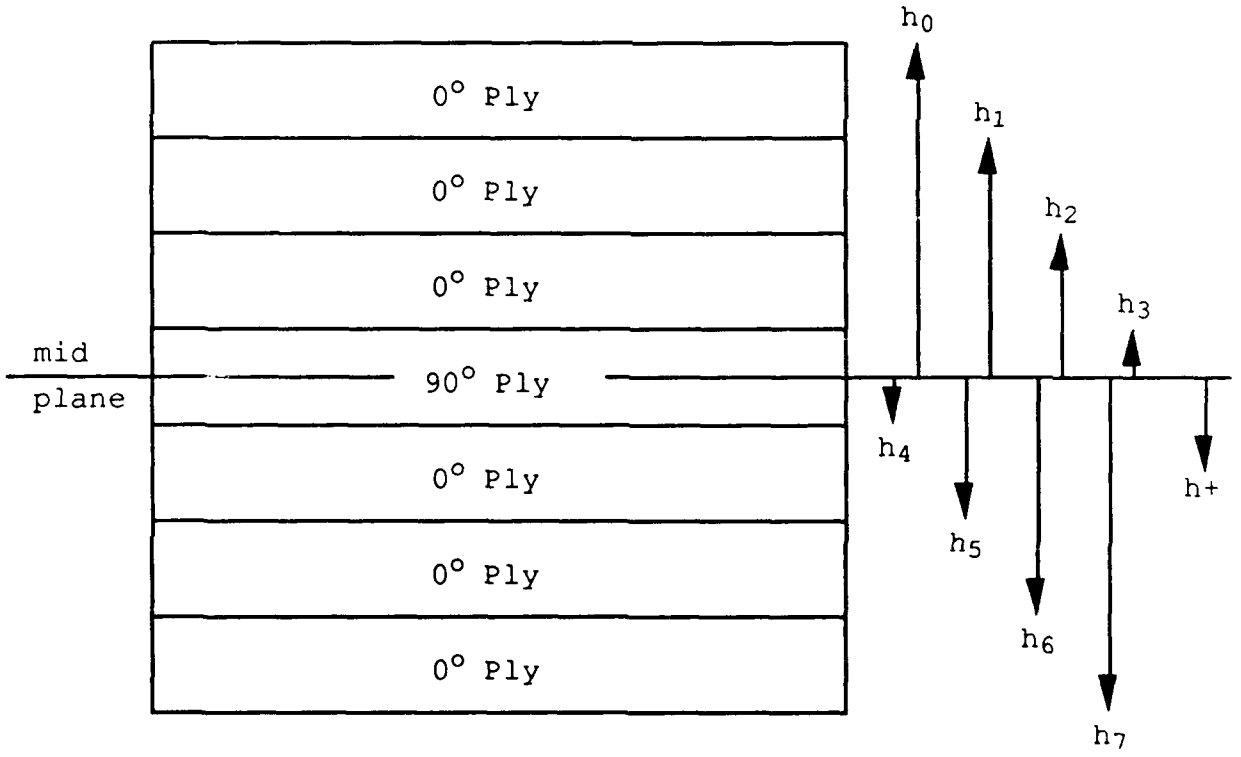

Figure 40. Laminate Geometry for First Ply Failure Calculations

Using Eqs (7-9), [A] (the extensional stiffness), [B] (the coupling stiffness) and [D] (the bending stiffness) are

$$[A] = [\bar{Q}]_0(h_3 - h_0) + [\bar{Q}]_{90}(h_4 - h_3) + [\bar{Q}]_0(h_7 - h_4)$$

$$[A] = \begin{bmatrix} 1373.57 & 164.12 & 0 \\ 164.12 & 988.74 & 0 \\ 0 & 0 & 446.67 \end{bmatrix} \text{ kips/in}$$

$$[B] = \frac{[\bar{Q}]_0}{2}(h_3^2 - h_0^2) + \frac{[\bar{Q}]_{90}}{2}(h_4^2 - h_3^2) + \frac{[\bar{Q}]_0}{2}(h_7^2 - h_4^2)$$

$$[B] = \begin{bmatrix} 0 & 0 & 0 \\ 0 & 0 & 0 \\ 0 & 0 & 0 \end{bmatrix}$$

$$[D] = \frac{[\bar{Q}]_0}{3}(h_3^3 - h_0^3) + \frac{[\bar{Q}]_{90}}{3}(h_4^3 - h_3^3) + \frac{[\bar{Q}]_0}{3}(h_7^3 - h_4^3)$$

$$[D] = \begin{bmatrix} 0.5917 & 0.0670 & 0 \\ 0.0670 & 0.3730 & 0 \\ 0 & 0 & 0.1824 \end{bmatrix} \text{ kipsin}$$

Then using Eqs (10-14),

$$[D_1] = \begin{bmatrix} 1.7253 & -0.3100 & 0 \\ -0.3100 & 2.7371 & 0 \\ 0 & 0 & 5.4828 \end{bmatrix} \frac{1}{\text{kipsin}}$$

$$[C_1] = \begin{bmatrix} -7.4276 & 1.2329 & 0 \\ 1.2329 & -10.30 & 0 \\ 0 & 0 & -22.40 \end{bmatrix} \times 10^{-4} \quad \frac{1}{kip}$$

$$[A_1] = \begin{bmatrix} 7.4276 & -1.2329 & 0 \\ -1.2329 & 10.30 & 0 \\ 0 & 0 & 22.40 \end{bmatrix} \times 10^{-4} \quad \frac{in}{kip}$$

Because the specimen is under uni-axial tension, the applied load can be written

$$[N] = \begin{bmatrix} N_x \\ 0 \\ 0 \end{bmatrix} \quad \frac{kips}{in}$$

where N_x is the applied stress in ksi times the thickness (approximately 0.07 in for $0_3/90/0_3$). The value of N_x which results in a stress in the 90° ply that exceeds the strength of the 90° ply is the stress that will cause first ply failure. Because the strength of the 90° ply is known (2.769 ksi), a solution for N_x can be found by iteration.

The mid-plane strain (the strain at the middle of the 90° ply) is found from Eq (15)

$$\boldsymbol{\varepsilon} = [A_1] \cdot [N] \tag{15}$$

The resulting stress in the 90° ply is

$$\boldsymbol{\sigma}_{90} = [Q]_{90} \cdot \boldsymbol{\varepsilon} \tag{19}$$

The iteration procedure is to pick a value for N_x in Eq (15), solve for ε, and then use Eq (19) to solve for the stress in the 90° ply. When the value for σ_{90} in Eq (19) is equal to 2.769 ksi, the proper value of N_x has been found.

For the $0_3/90/0_3$ lay-up, N_x = 0.29508 kip/in was found to give σ_{90} = 2.769 ksi. Thus, the first ply failure would occur at an applied stress of

$$\sigma_{fpf} = \frac{0.29508 \text{ kip/in}}{0.07 \text{ in}} = 4.22 \text{ ksi}$$

Using a similar procedure, the first ply failure stresses for the other three lay-ups were determined.

B. Predicted Modulus of Elasticity Calculations

Using Eq (20) and the results of the first ply failure predictions, the predicted modulus of elasticity was determined as follows:

$$E = \frac{1}{(t)A_{1_{11}}} = \frac{1}{(0.07 \text{ in})(7.4276 \times 10^{-4} \text{ in/kip})} = 19.23 \text{ msi}$$

The modulus of elasticity following first ply failure was predicted using the ply discount method. Thus, $[\bar{Q}]_{90}$ was set equal to zero and a new $[A_1]$ matrix was formed. For the $0_3/90/0_3$ lay-up, the new $[A_1]$ matrix was

$$[A_1] = \begin{bmatrix} 8.2102 & -1.4778 & 0 \\ -1.4778 & 13.100 & 0 \\ 0 & 0 & 26.10 \end{bmatrix} \times 10^{-4} \quad \frac{in}{kip}$$

and the modulus following first ply failure was

$$E = \frac{1}{(t)A_{1_{11}}} = \frac{1}{(0.07\ in)(8.2101 \times 10^{-4}\ in/kip)} = 17.40\ msi$$

A similar procedure was followed to determine the modulus after first ply failure for the other three lay-ups.

Bibliography

1. Garrett, K. W. and Bailey, J. E., "Multiple Transverse Fracture in 90° Cross-Ply Laminates of a Glass Fibre-Reinforce Polyester," *Journal of Materials Science*, 12: 157-168 (1977).

2. Parvizi, A., Garrett, K. W. and J. E. Bailey. "Constrained Cracking in Glass Fiber-Reinforced Epoxy Cross-Ply Laminates," *Journal of Materials Science*, 13: 195-201 (1978).

3. Wang, S. W. and A. Parvizi-Majidi. "Mechanical Behavior of Nicalon Fiber Reinforced Calcium Aluminosilicate Matrix Composites," presented at *The 14th Annual Conference on Composites and Advanced Ceramic Materials*, Cocoa Beach, FL (January 1990).

4. Kim, Ran Y. and N. J. Pagano. "Initiation of Damage in Unidirectional Brittle Matrix Composites," *Proceedings of the 4th Japan-US Conference of Composite Materials*, Washington, D.C.: 799-812 (June 1988).

5. Sun, C. T. and K. C. Jen. "On the Effect of Matrix Cracks on Laminate Strength," *Journal of Reinforced Plastics and Composites*, Vol. 6, No. 3, July 1987: 208-222.

6. Reifsnider, K. L., Henneke, E. G. and W. W. Stinchcomb. "Defect-Property Relationships in Composite Materials," *AFML-TR-76-81, Part IV*. Air Force Materials Laboratory (June 1979).

7. Talreja, Ramesh. *Fatigue of Composite Materials*. Lancaster, PA: Technomic Publishing Company, 1987.

8. Jones, Robert M. *Mechanics of Composite Materials*. New York: Hemisphere Publishing Corporation, 1975.

9. Laws, Norman and George J. Dvorak. "Progressive Transverse Cracking In Composite Laminates," *Journal of Composite Materials*, Vol. 22, No. 10, October 1988: 900-916.

10. Wang, A. S. D., and F. W. Crossman. "Initiation and Growth of Transverse Cracks and Edge Delamination in Composite Laminates Part 1. An Energy Method," *Journal of Composite Materials*, Supplement, Vol. 14, 1980: 71-87.

11. Vozzola, R. P. *Fracture Toughness Testing of a Ceramic Matrix Composite*. MS thesis, AFIT/GAE/AA/87D-24. School of Engineering, Air Force Institute of Technology (AU), Wright-Patterson AFB, Ohio, December 1987.

12. Zawada, L. P., ceramics engineer, Metals and Ceramic Division, Wright Research and Development Center. Personal interviews. WRDC/MLLN, Wright-Patterson AFB, Ohio, 28 Mar. - 12 Oct. 1990.

13. Fink III, Capt Walter E. *Investigation of Failure Modes in a Ceramic Composite Under Off-Axis Loading*. MS Thesis, AFIT/GAE/ENY/89D-9. School of Engineering, Air Force Institute of Technology (AU), Wright-Patterson AFB OH, December 1989.

14. Mall, S., and R. Y. Kim. "Damage Initiation and Growth in a Quasi-Isotropic Laminate of Ceramic Matrix Composite," *Proceedings of the 1990 SEM Spring Conference on Experimental Mechanics*, Albuquerque, New Mexico: 732-737 (June 1990).

15. Kim, Ran Y. "Fatigue Behavior" in *Composites Design*, ed. Stephen W. Tsai. Dayton, OH: Think Composites, 1987.

Vita

Captain Steven E. Bachmann [redacted] graduated from Poquoson High School, Poquoson, Virginia in 1981. He attended the University of Virginia, from which he received a Bachelor of Science Degree in Aerospace Engineering in May 1985. Upon graduation, he received a commission in the USAF through the ROTC program. He was assigned to the F-16 System Program Office at Wright-Patterson AFB, Ohio as the reliability and life cycle cost program manager for the F-16. He served in this capacity until entering the School of Engineering, Air Force Institute of Technology, in May 1989.

[redacted]

REPORT DOCUMENTATION PAGE

Form Approved
OMB No 0704-0188

1. AGENCY USE ONLY (Leave blank)	2. REPORT DATE	3. REPORT TYPE AND DATES COVERED
	Dec 1990	Master's thesis

4. TITLE AND SUBTITLE

Transverse Cracking in a Fiber Reinforced Ceramic Matrix Composite

5. FUNDING NUMBERS

6. AUTHOR(S)

Steven E. Bachmann, Capt, USAF

7. PERFORMING ORGANIZATION NAME(S) AND ADDRESS(ES)

Air Force Institute of Technology
WPAFB, OH 45433-6583

8. PERFORMING ORGANIZATION REPORT NUMBER

AFIT/GAE/ENY/90D-2

9. SPONSORING/MONITORING AGENCY NAME(S) AND ADDRESS(ES)

Dr. Ted Nicholas
WRDC/MLLN
WPAFB, OH 45433

10. SPONSORING/MONITORING AGENCY REPORT NUMBER

11. SUPPLEMENTARY NOTES

12a. DISTRIBUTION AVAILABILITY STATEMENT

Approved for public release;
distribution unlimited

12b. DISTRIBUTION CODE

13. ABSTRACT (Maximum 200 words)

The purpose of this study was to investigate the transverse cracking behavior of a fiber reinforced ceramic matrix composite. The major objectives were to determine the crack initiation stress and the minimum transverse crack spacing for different cross-ply lay-ups of SiC/1723, to provide explanation for the differences in the performance of the lay-ups, and to compare the test results to available theoretical models and to other composite systems.

The thickness of the transverse ply was found to have a great effect on the transverse cracking behavior of the laminates. The saturation crack spacing decreased as the transverse ply thickness was decreased and for a given strain, the crack spacing increased as the transverse ply thickness was increased. The strain for the onset of transverse cracking increased as the transverse ply thickness was decreased.

Classical laminate theory was used to predict crack initiation stresses and modulus of elasticity. A crack spacing theory based on shear lag analysis was applied. Comparisons were made to glass/epoxy and graphite/epoxy systems.

14. SUBJECT TERMS	15. NUMBER OF PAGES
composite, transverse cracking, ceramic, fiber, crack density, matrix	109
	16. PRICE CODE

17. SECURITY CLASSIFICATION OF REPORT	18. SECURITY CLASSIFICATION OF THIS PAGE	19. SECURITY CLASSIFICATION OF ABSTRACT	20. LIMITATION OF ABSTRACT
unclassified	unclassified	unclassified	UL